MODELING FLUID FLOW THROUGH A SINGLE FRACTURE USING EXPERIMENTAL, STOCHASTIC, AND SIMULATION APPROACHES

A Thesis

by

DICMAN ALFRED

Submitted to the Office of Graduate Studies of
Texas A&M University
in partial fulfillment of the requirements for the degree of

MASTER OF SCIENCE

December 2003

Major Subject: Petroleum Engineering

MODELING FLUID FLOW THROUGH A SINGLE FRACTURE USING EXPERIMENTAL, STOCHASTIC, AND SIMULATION APPROACHES

A Thesis

by

DICMAN ALFRED

Submitted to Texas A&M University
in partial fulfillment of the requirements
for the degree of

MASTER OF SCIENCE

Approved as to style and content by:

David S. Schechter (Chair of Committee)	Jerry L. Jensen (Member)
Robert R. Berg (Member)	Hans C. Juvkam-Wold (Head of Department)

December 2003

Major Subject: Petroleum Engineering

ABSTRACT

Modeling Fluid Flow Through a Single Fracture Using Experimental, Stochastic, and Simulation Approaches. (December 2003)

Dicman Alfred, B.Tech., Indian Institute of Technology

Chair of Advisory Committee: Dr. David S. Schechter

This research presents an approach to accurately simulate flow experiments through a fractured core using experimental, stochastic, and simulation techniques. Very often, a fracture is assumed as a set of smooth parallel plates separated by a constant width. However, the flow characteristics of an actual fracture surface are quite different, affected by tortuosity and the impact of surface roughness. Though several researchers have discussed the effect of friction on flow reduction, their efforts lack corroboration from experimental data and have not converged to form a unified methodology for studying flow on a rough fracture surface.

In this study, an integrated methodology involving experimental, stochastic, and numerical simulations that incorporate the fracture roughness and the friction factor is shown to describe flow through single fractures more efficiently. Laboratory experiments were performed to support the study in quantifying the flow contributions from the matrix and the fracture. The results were used to modify the cubic law through reservoir simulations. Observations suggest that the fracture apertures need to be distributed to accurately model the experimental results.

The methodology successfully modeled fractured core experiments, which were earlier not possible using the parallel plate approach. A gravity drainage experiment using an X-ray CT scan of a fractured core has also validated the methodology.

DEDICATION

To my beloved parents, Alfred and Mangayarkarasi, my chellam, and my teachers and mentors in college.

ACKNOWLEDGMENTS

I would like to take this opportunity to express my deepest gratitude and appreciation to the people who have given me their assistance throughout my studies and during the preparation of this thesis. I would especially like to thank my advisor and committee chair, Dr. David S. Schechter, for his continuous encouragement, financial support, and especially for his academic and creative guidance. He has been my source for inspiration throughout my graduate studies.

I would like to thank Dr. Jerry L. Jenson and Dr. Robert R. Berg for serving as committee members, and I do very much acknowledge their friendliness, guidance, and helpful comments while working towards my graduation. I wish to thank Dr. Tom Blasingame and Dr. C. Bowman, former Head of the Department, for selecting me to receive the Texaco Fellowship through the Harold Vance Department of Petroleum Engineering. This support was clearly one of the most significant events of my college education, and indeed very helpful in order to pursue my professional career. Also, I really do appreciate the help and support I received from my undergraduate advisor, Dr. T. Sunderrajan.

I wish to take the opportunity to thank and acknowledge Dr. Erwinsyah Putra, who is my mentor and guiding light in this research. I know in my heart that I would not be where I am today without the guidance I received from him. I do very much acknowledge his friendship, guidance, and patience throughout my graduate program.

I would also like to thank Zuher Syihab for our memorable friendship and for his guidance and support. Finally, I want to thank my friends in the naturally fractured reservoir group, Tanvir (now with Object Reservoir), Goke (now with Shell), Vivek Muralidharan, Sandeep Kaul, Prasanna, Mirko, Babs, Jeff, Jesus and Kim. I would also like to thank Pepe, Manoj, Harshal, Priya, Shey and my roomies Woodi, Anunay, Sharat, Vijay for making my graduate years very pleasant. The facilities and resources provided by the Harold Vance Department of Petroleum Engineering are gratefully acknowledged. I thank Texas A&M University for educating me in various ways, and for providing me

with the very best education there is. I would like to take the opportunity to thank the faculty and staff helping me prepare for a life after graduation.

I am going to remember these years of hard work with great pleasure. To all of you, I appreciate what you have done to help me in my scholastic and professional growth. I would like to thank you for providing me with a work environment that lends itself to creativity and productivity, without too much financial concern. Not everyone is so fortunate. I know I still have much to learn, but with continued support and encouragement from people like you I know I can accomplish a great deal.

Thank you very much.

TABLE OF CONTENTS

Page

LIST OF FIGURES

FIGURE Page

FIGURE Page

LIST OF TABLES

CHAPTER I

INTRODUCTION – FLUID FLOW THROUGH SINGLE FRACTURES

The search for hydrocarbons has been expanded into the harder-to-evaluate formations, where potential hydrocarbon reserves maybe located. The naturally fractured reservoirs stand out as a prime candidate among them. Over the past few years, extensive studies have been conducted on fractured reservoirs, because they are difficult to simulate due to the complexity of fractured reservoirs and also the presence of tectonic discontinuities. The production capabilities have been restricted because of the lack of knowledge about the fractures and the flow, which occurs through fractures. Understanding the fluid flow characteristics of fractures is very important to model flow through fractures and hence extend it to the behavior of the reservoir. Fracture aperture and connectivity are the most critical properties controlling flow and contaminant transport in the saturated zone. This is because under laminar flow the transmissivity of a planar smooth-sided fracture is very sensitive to aperture size. Transmissivity is found to be proportional to the cube of the aperture. This is known as the "cubic law" of fracture flow. [1]

A parallel plate model is widely used to simulate flow in a fracture due to its simplicity of idealizing a fracture. However, a real fracture has characteristics of variable aperture in nature. Due to the large flow capacity of a fracture, water flow through the fracture plays a significant role in overall oil recovery of fractured reservoirs. Despite the success of waterflooding to improve oil recovery in a fractured rock, the understanding of true mechanism and a numerical simulation of water injection are not sufficient. Waterflooding in the naturally fractured reservoirs of West Texas (Spraberry Trend Formation) failed due to lack of understanding of the fracture flow and the connectivity issues associated with it.[2]

The parallel plate model is still widely adopted in petroleum engineering because of its simplicity of idealizing a fracture. In case of a parallel plate model, invading

---

This thesis follows the style of the *Journal of Petroleum Technology*.

waterfront is evenly distributed over the fracture plane and water can access to all interfaces between the fracture and the matrix.[3]

However, flow on a real fracture surface is very unevenly distributed along the fracture plane. Therefore, the parallel plate approach is inadequate in describing flow through the fracture.

In a real fracture, the phases are unevenly distributed and is governed by complex processes such as phase isolation and pinching off of nonwetting phase globules.[4,5] The importance of fracture heterogeneity on mass transfer between matrix and fracture can be found in the work of Firoozabadi and Tan.[6]

Fracture permeability is usually estimated by a cubic law that is based on the theory of hydrodynamics for the laminar flow between flat plates. However, the cubic law is too simple to estimate the fracture permeability correctly, because the surface of real fracture is much more complicated and rougher than the surface of flat plate. Several researchers have shown that the flow characteristics of an actual fracture surface would be quite different due to the effect of tortuosity, impact of surface roughness and contact areas. Nonetheless, to date, these efforts have not converged to form a unified definition on the fracture aperture applied through cubic law.

1.1 Literature review

Early investigators based their idea that a parallel plate concept would be utilized to understand the concept of fluid flow through fractures. The first comprehensive work on flow through open fractures was done by Lomize.[7] He used parallel glass plates and demonstrated the validity of cubic law as long as the flow was laminar. He also investigated the effects of changing the fracture walls from smooth to rough and, finally, to model with different fracture shapes. He introduced the concept of defining the surface roughness based on empirical data. Later he developed a flow regime chart that takes into account the effects of roughness and turbulent flow in open fractures. He proposed to include the roughness factor into the flow equation. It was Snow [8] who used this concept to simulate real fractures. The cubic law governs the viscous flow through a fracture with smooth and parallel walls. He discussed about the need for careful assessment since real

joints in rock does not represent the parallel plate model assumed then. With this idealization he treated flow along intersecting fractures as being proportional to the cubic of the apertures.

Iwai[1] conducted a comprehensive study of fluid flow through a single fracture and investigated the validity of the cubic law. One of the important features of his experiments was that the fracture planes had contact area as well as roughness. Utilizing this observation, an idealized fracture model can be constructed in which flow paths are represented by an opening which varies continuously normal to the flow but with constant aperture in the flow direction.

Nuezil and Tracy[9] modeled fracture flow, by representing fractures as a set of parallel openings with different apertures. They generated an aperture distribution through a lognormal distribution and studied the flow through numerical analysis. They showed that the flow conformed to the cubic law and also that the maximum flow occurs through the largest apertures, thereby emphasizing that flow occurs through preferred paths. Thus in their analysis, the flow depended on the tail of the frequency distribution. Witherspoon *et al.*[10] stated that cubic law was found to be valid whether the fracture surfaces were held open or were being closed under stress, and the results were independent of rock type. Permeability was uniquely defined by fracture aperture and was independent of the stress history. The effects of deviations from the ideal parallel plate concept only caused an apparent reduction in flow and may be incorporated into the cubic law by a flow modification factor.

Tsang and Witherspoon[11] studied the dependence of mechanical and fluid flow properties of a fracture on its roughness and sample size. They correlated the shape of the aperture distribution to the specific fractures of the stress-strain behavior and also to the fluid flow characteristics. Theoretical and experimental studies of fracture geometry have shown that the parallel plate model does not accurately depict a rock fracture. For example, Tsang and Witherspoon[11] present figures of actual fracture profiles derived from Bandis *et al*. [12] These fracture profiles are non-parallel and consist of both a large-scale undulation and small-scale roughness.

Tsang *et al*. [13] investigated the effect of tortuosity in fluid flow through fractures and found that it plays a significant role. He represented the flow paths with electrical resistors placed in a 2 dimensional grid. Fracture apertures obtained from both laboratory and from hypothetical analytic function were used in the study. He found out that, the more small apertures are present in the aperture distribution, the more the effect of tortuosity. He related the increase in tortuosity and the decrease in connectivity of the fluid flow paths to the increase in fracture contact area. Though he did not model the effect of surface roughness with actual flow experiments, he stated that the tortuosity along with the effect of surface roughness depresses the flow rate from the value predicted by the parallel plate theory by three or more orders of magnitude.

Brown[14] investigated the effect of surface roughness on fluid flow through rock joints. He observed that the deviations of fluid flow from the cubic law could merely stem from the fact that the surfaces are rough and contact each other at discrete points. He performed a simulation of flow between rough surfaces using a fractal model of surface topography. The solution was the local volume flow rate through the rock joint. He solved this flow rate to derive the "hydraulic aperture" using the cubic law. When actual fracture aperture measurements are not possible, hydraulic or equivalent fracture aperture width is utilized to define flow properties. In this research equivalent aperture width is calculated using flow experiments. Brown concluded that for small aperture separation the topography did have a significant effect through tortuosity, as stated by many researchers. And also he found out that the parameter most affecting the fluid flow through rock joints is the ratio of the mean separation between the surfaces to the root mean square surface height. This parameter describes the nature of the roughness that protrudes into the fluid and accounts for most of the disagreement with the parallel plate model. This finding was further established in our research work.

Tsang and Tsang [15] developed a conceptual model to effectively model flow channels for fractured media. They employed a log normal distribution and generated a statistical aperture distribution based on the mean, variance and spatial correlation length. They made predictions for tracer breakthrough curves in case of single fracture with varying overburden stress based on their conceptual model, which seem to correspond

well with the one provided by Moreno *et al*.[16] They also expressed the importance of laboratory experiments to validate their model.

Work by other researchers show that the flow through a fracture follows preferred paths or flow channels due to the variation in fracture aperture.[9,14-18] One aspect, which everybody agrees is that the fractures are not parallel walls but are themselves 2-dimensional networks of variable aperture. Hence, fluid flow in single fractures probably does not strictly follow the cubic law.

The focus of this research is to understand and quantify these deviations from the cubic law. Also these investigations were associated with open fractures, and, of course, one will encounter many situations in the field where the fractures are not open. Usually, fracture surfaces have some degree of contact, and the effective aperture will depend upon the normal stresses acting across the discontinuity. But since a part of the flow is blocked by asperities, there were concerns whether the cubic law would actually be valid. Several researchers have proposed a new model wherein the fracture is represented by a set of parallel plate openings with different apertures. The model leads to a modified Poiseuille equation for flow, which includes an aperture frequency distribution for the fracture.[18]

In the last two decades, researchers have employed more realistic description of a rock joint with a range of apertures and the impact of the aperture variation with a single rock joint on its flow properties has been recognized.[11,13,14] The techniques used in the industry to obtain aperture measurements include 1) joint surface profiling 2) low melting point metal injection 3) resin casting technique. These measurements have provided useful and important data for the basic studies of flow and transport through variable-aperture fractures. However, in practical field problems it is neither feasible nor practical to make such detailed measurements of apertures in all fractures participating in the flow and transport. Furthermore aperture measurements of exposed fractures at the borehole walls, tunnel walls of core samples may be affected by the drilling or evacuation process so that they may not be representative of the fractures in the rock mass.[19]

Tsang and Tsang [15] chose a statistical description of a fracture with variable apertures by means of three parameters, two related to the aperture distribution: mean

aperture and the standard deviation, and one to the spatial arrangement of the aperture, the spatial correlation length. This was similar to their previous study [18] where they generated fracture aperture distribution by the same means and through simulation study. They concluded that the majority of the flow tends to be concentrated in certain preferred paths. They performed numerical flow and transport experiments with them with particular emphasis of correlate the fracture geometry parameters with observed measurable hydrological quantities. Though they advocated the need for this kind of hydrological measurements and interpretation they concluded that the correspondence between observations and the hydrological properties is still ambiguous.

For the purpose of supporting the fracture model, laboratory experiments have been conducted in this research. The process of experiments involved establishing fracture permeability changes at various confining pressures and then quantifying flow contributions from the matrix and the fracture. Fractured core experiments were conducted with varying over burden pressures in order to calculate different aperture widths, which would further bolster the fracture model established through simulations.

The reduction in permeability with overburden pressure has been well known. Fatt and Davis[19] presented the changes in permeability with pressure at range 0 to 15,000 psig and found that overburden pressure caused a reduction in permeability of the consolidated oil-bearing sandstone samples by as much as 50 per cent at 10,000 psig. Wyble[20] performed similar experiments on three different sandstone samples to determine the changes in conductivity, porosity and permeability at pressure range 0 to 5,000 psig. His results were consistent with the observations by Fatt and Davis.[19] During the experiments, different overburden pressures (radial force) were applied only to the cylinder core while the axial direction was kept at constant atmospheric pressure.

Gray *et al.*[21] enhanced the previous experiments by applying axial force and combining with overburden pressure (radial force) to measure the anisotropy permeability changes at more representative reservoir stress-state condition. They showed that permeability reduction subjected to overburden pressure as a function of the ratio of radial to axial stress and the permeability reduction under non-uniform stress (radial pressure ≠ axial pressure) is less than that under uniform stress.

Although extensive work has been established on the effect of overburden pressure[22] and stress-state on matrix permeability[23] but there are some very interesting details of fractured rock behavior under stress that have not been investigated.

1.2 Motivation and objective

Although several researchers have analyzed the fracture flow and its deviations from the cubic law in great detail, none of them provide a definite picture of modeling both rough surfaces and the roughness factor associated with it. Except for Brown [14] none have tried to quantify the reduction in flow rates as a result of tortuosity due to rough surfaces. And also his studies did not involve flow experiments rather he observed the phenomenon using resistors. The conceptual models developed in the past have not been corroborated through laboratory results. The focus of this research is to prove that accurate results could be obtained from cubic law if modified to account for the effect of roughness. Though several papers have discussed the effect of friction in flow considerations, the application of friction factor into simulations have not been looked into with reference to the experimental results. This stimulates the current effort to develop a general model for simulating flow through fractures by incorporating the friction factor or the flow modification factor to alter the fracture permeability distribution on the surface of the fracture.

1.3 Methodology

In this research experiments were performed with a fractured core to study the flow behavior in fractures with increasing overburden pressures. The objective of these type of experiments is to quantify the variation of aperture widths with different overburden pressure. The laboratory measurements were analyzed and an effective fracture aperture width was inferred using cubic law. Then a two dimensional network of fracture aperture distribution was generated using stochastic analysis (lognormal distribution), following similar approaches by earlier researchers. The effect of surface roughness on flow was accounted for by means of a friction factor to obtain a modified permeability distribution in a fracture. The fracture permeability distribution modified for local roughness was then imported to a commercial simulator to simulate the experiments. From the modeling it is

evident that single fracture of constant aperture fails to model the experimental results and hence the cubic law. The goal of this research is to examine the effect of surface roughness for flow through fractures and to effectively incorporate them into simulations with the aid of geostatistics. Since this research has been supported with experimental results, the consistency of the results enabled us to define a methodology for single fracture simulation.

CHAPTER II

EXPERIMENTAL ANALYSIS TO QUANTIFY FRACTURE APERTURES AND FLOW CONTRIBUTION FROM MATRIX AND FRACTURE UNDER VARYING CONFINING PRESSURES

2.1 Experimental procedure

For many years efforts have been performed in the laboratory experiments to duplicate the reservoir conditions. In this study, the permeability changes at different overburden conditions are investigated. For simplicity and the difficulty of applying force in the axial direction, these experiments assume the axial direction is in the atmospheric pressure. Thus, only overburden pressure generated from hydraulic jack was applied to cylindrical face of the core. (Fig. 2.1)

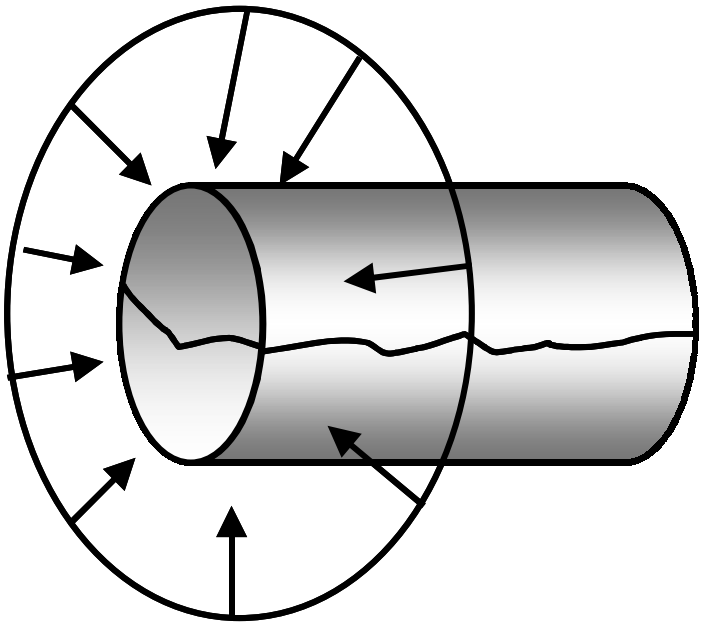

Figure 2.1 – Illustration of the confining pressure applied on the core.

Synthetic brine was used in the experiments. The brine contains NaCl and $CaCl_2.H_2O$ mixed with distilled water. The clean core was saturated with brine then it was inserted into a Hassler-type core holder using a confining pressure of 500 psia. Then, core flooding was performed with different injection rates. After running set of injection rates at this pressure, we changed to other confining pressures and performed with different injection rates again. Similar procedure was performed using fractured core. Details of procedure for conducting core flooding experiments can be found in Appendix-A. The procedure can be used for single and two phase experiments. The current results are from the single-phase experiments. The experimental set up is shown in Fig. 2.2.

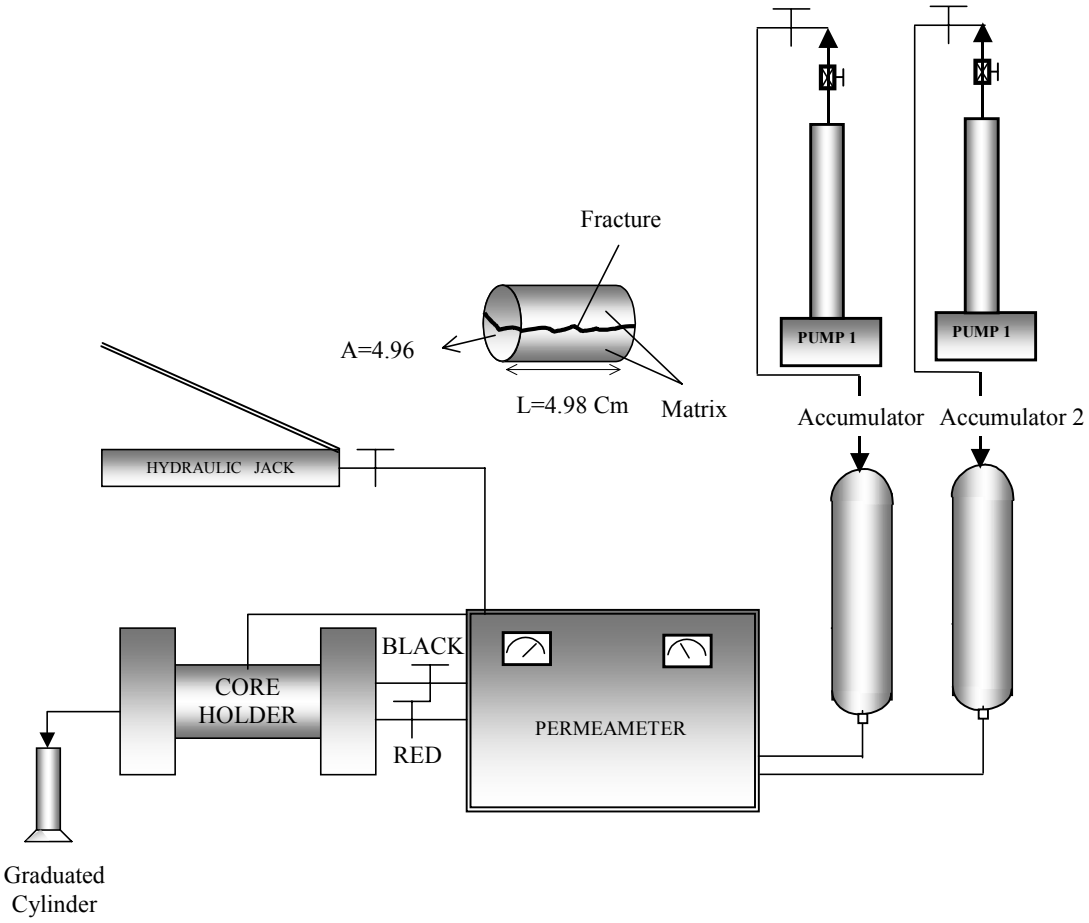

Figure 2.2 - Schematic diagram of the two-phase core flooding experiment.

A Berea core was used during the core flooding experiments. The core properties are given in the note remark of Table 2.1. Two sets of injection rates ranging from 5 cc/min to 20 cc/min were performed at each overburden pressure. Three different overburden pressures were applied started from 500 to 1500 psia as listed in Tables 2.1 and 2.2 for both unfractured and fractured Berea core. The core was cut using a hydraulic cutter to generate fracture horizontally along the axis of the core. During the experiments using a fractured core, the pressure drop across the core is lower and the core permeability increases about 3 times higher compared to those obtained using unfractured core.

Table 2.1- Experimental observations for unfractured core.

Pob **psia**	Δp **psia**	k_m **md**	Q **cm^3/min**
485.7	4.1	299.7	5
506.4	8.1	303.4	10
502.9	12.4	297.2	15
504.4	16.5	297.85	20
501.0	4.2	292.5	5
504.9	8.5	289.0	10
501.0	13.0	283.0	15
502.0	17.0	289.1	20
1000.4	4.5	273.0	5
1002.4	9.0	273.0	10
1000.5	13.7	269.0	15
1000.5	18.2	270.0	20
1000.2	4.8	255.9	5
1003.5	9.7	253.3	10
1002.7	14.5	254.2	15
1004.1	19.2	255.96	20
1500.0	5.1	240.8	5
1500.0	10.4	236.3	10
1500.7	16.4	224.7	15
1503.1	22.1	222.4	20
1500.3	5.5	223.4	5
1501.0	11.2	219.4	10
1501.3	17.3	213.0	15
1502.3	22.7	216.5	20

NOTE:	
Berea Core Properties	
Length	4.9784 Cm
Diameter	2.5146 Cm
Viscosity	1.0 Cp
Area	10.9637 Cm^2
Porosity	23.58 %

Table 2.2- Experimental observations for fractured core.

Pob psia	Δp psia	k_{av} md	Q cm^3/min
501.3	1.4	877.5	5
500.2	2.8	877.6	10
503.3	4.1	898.9	15
503.3	5.4	910.0	20
494.8	1.0	1228.7	5
509.4	2.6	945.1	10
508.8	4.2	877.6	15
509.6	5.8	847.3	20
970.5	2.2	558.4	5
1000.5	4.8	511.9	10
1001.0	7.6	485.0	15
1016.7	11.3	434.9	20
1000.8	2.3	534.0	5
1002.2	5.8	423.6	10
1009.7	9.1	405.0	15
1002.7	13.9	353.6	20
1500.3	4.2	292.5	5
1504.6	9.3	268.2	10
1507.9	15.1	244.1	15
1504.8	21.4	229.6	20
1500.7	5.0	245.7	5
1506.0	10.9	225.4	10
1509.6	17.4	211.8	15
1509.6	22.5	218.4	20

Figure 2.3 shows that the effect of varying overburden pressures on unfractured core is not significant in contrast with that effect on fractured core. The average permeability of fractured core significantly reduces and tends toward the permeability of unfractured core at 1500 psia. The trend lines are used to illustrate this phenomenon and not for any calculation purposes. The result suggests that the effect of stresses may be most pronounced in fractured reservoirs where large pressure changes can cause significant changes in fracture aperture and the related changes in conductivity within a reservoir as mentioned by Lorenz [22].

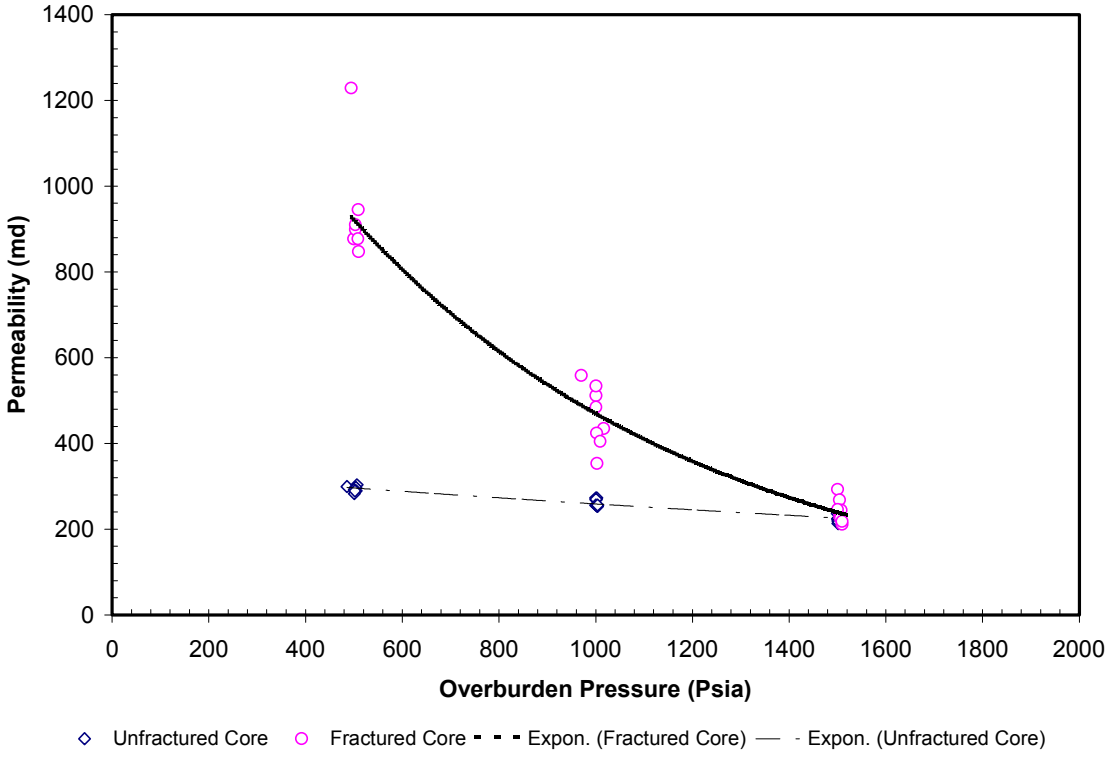

Figure 2.3 – Comparison permeability reduction between unfractured and fractured cores due to increasing overburden pressure.

2.2 Data analysis

In order to properly quantify the effect of fracture permeability on the fluid flow, it is important to describe the equations describing the changes of this parameter under different overburden pressure. The equations governing the fluid flow through fractures have been widely published in the reservoir engineering literature and are not discussed here. However, the pertinent equations used for our analysis are presented as follows:

The fracture permeability, k_f, is obtained by combining the viscous force and Darcy equation for flow through fractures as given below,

$$k_f = 8.45\times10^9\, w^2 \qquad (1)$$

where w is fracture width in centimeters and k_f is in millidarcies.

Fracture width is a function of fracture permeability and those two parameters are unknown. To obtain those parameters, one more equation is needed.

We obtained the average permeability of fracture and matrix, k_{av}, from core flooding experiments using a fractured core and matrix permeability, k_m, using unfractured core. Thus, another fracture permeability equation can be obtained following this equation below.

$$k_f = \frac{k_{av}A - k_m(A - wl)}{wl} \tag{2}$$

where A is matrix area (cm^2), k_f is fracture permeability(cm^2) and l is diameter of the core (cm).

The assumption in the above equation is that once the core is fully saturated (single phase), the flow through the fracture and the matrix is independent of each other. Now, there are two equations and two unknowns. So, combining equations 1 and 2 can solve the fracture permeability and fracture width. First, the equation 3 is applied to solve w then it is inserted to equation 1 to solve k_f.

$$8.45\times10^9 w^3 l - k_{av}A + k_m(A - wl) = 0 \tag{3}$$

It is also important to determine the contribution flow rate from the matrix (q_m) and fracture (q_f). The contribution from each zone is determined by applying Darcy's equations. The equation for flow rate in matrix is:

$$q_m = \frac{k_m A \Delta p}{\mu L} \tag{4}$$

where q_m is the matrix flow rate (cc/sec), k_m is the matrix permeability (Darcy), A is the matrix area (cm^2), Δp is pressure drop across the core (atm), μ is viscosity (cp) and L is core length (cm).

The flow through a smooth conduit can be expressed by involving the fracture width (w) and the pressure gradient (Δp):

$$q_f = 9.86\times10^9 \frac{w^3 l \Delta p}{12 \mu L} \quad (5)$$

where q_f is the fracture flow rate (cc/sec), w is the fracture width (cm), l is a lateral extend of the fracture (cm), Δp is pressure drop across the core (atm), μ is viscosity (cp) and L is core length (cm).

2.3 Artificially fractured core simulation

A numerical model utilizing commercial simulator (CMG™) was used to study the fluid flow through fracture at different overburden pressures. The laboratory process in which the water was injected through the fracture was duplicated in this modeling effort. The rectangular grid block was applied to overcome the difficulty of modeling a cylindrical core shape [2]. A 31x31 grid blocks were used in the x and z directions with 1 grid block in the y direction. The fracture layer is located only in the 16th layer and the rest are matrix layers. The permeability in fracture layer was calculated based on two parallel plates without fracture roughness. All the layers were injected with constant water injection of 5 cc/hr. At the opposite end, two production points were located in the matrix and fracture layers to quantify the amount of water produced at those two points.

In the experimental process, the core is saturated with the water. Once water injection was started with constant rate, water was produced simultaneously. Then the water that was produced from both matrix and fracture layers at the end point was recorded. In the simulation, however, the initial water saturation condition is assumed zero to visualize the movement of water through single fracture. The water saturation change in the matrix and fracture during transient state can be observed as illustrated in Fig. 2.4.

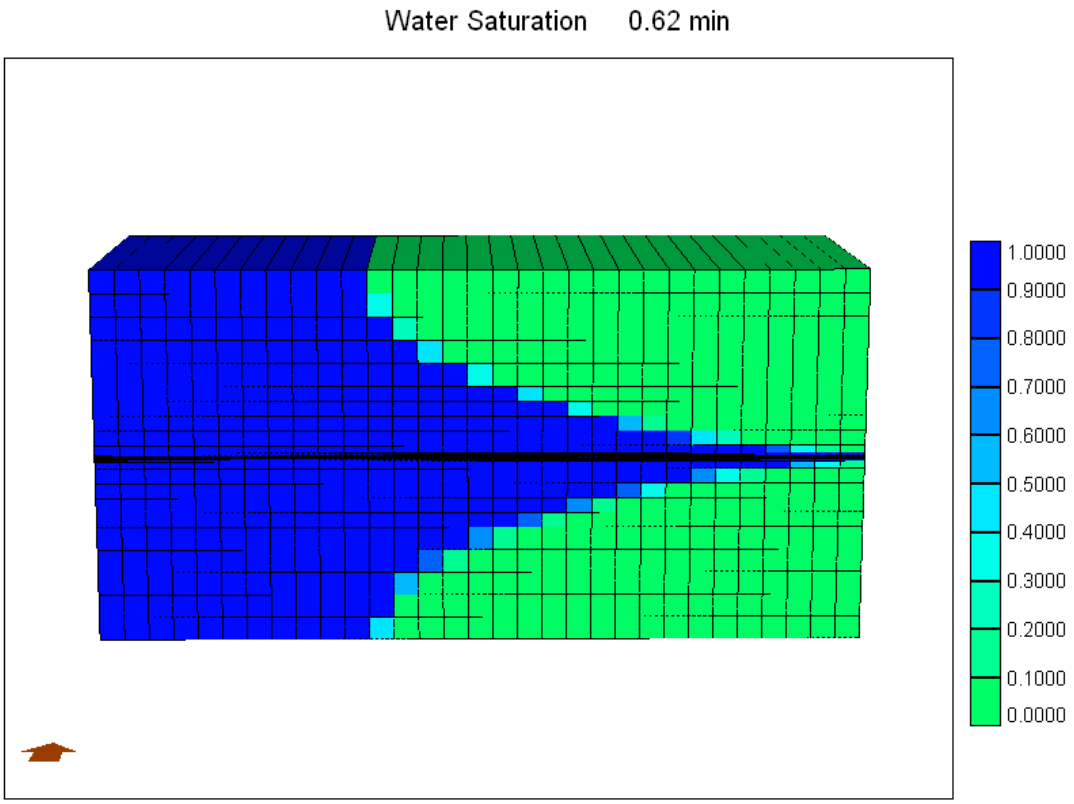

Figure 2.4 - Water saturation change in matrix and fracture at transient flow condition.

A few minutes after the injection was started, the flow rate was still in the transient condition and then reached a steady state condition at later time as shown in Fig. 2.5. At steady state condition, the amount of water produced from matrix and fracture was recorded. Similar simulation runs were performed for different overburden pressures.

2.4 Error analysis

Any experimental data are subject to errors. So an error analysis was performed using the experimental data to quantify the range of error in the calculation of matrix and fracture flow rates. The summary of the error analysis for the injection rate case of 5 cc/min is presented in Table 2.3. The parameter fracture flow rate (Q_f) in Table 2.3 was calculated by subtracting the matrix flow rate from the total injection rate. From the table we find that the errors involved in the calculation of fracture flow rates are relatively small (<

8%), at lower overburden pressures (500 and 1000 psia) when compared to the high overburden pressure case (1500 psia). This indicates that the values obtained at high overburden pressure have a high degree of uncertainty.

This could be due to the fact that at high overburden pressures, the characteristics of the matrix have a dominant influence on fracture flow. Due to time constraint, the high levels of uncertainty at higher overburden pressures have not been explored or taken into account while modeling. This is an area where more analysis could be done in the future.

Table 2.3- Experimental error analysis.

Overburden Pressure, psia	K_m, md	Pressure Drop psia	Q_m cc/min	Q_m cc/min		Q_f cc/min		Error in Q_f, %
				mean	Std dev	mean	Std dev	
500.00	max = 299.96	1.00	1.21	1.44	±0.27	3.56	±0.27	7.59
		1.40	1.70					
	min= 292.44	1.00	1.18					
		1.40	1.66					
1000.00	max = 273.02	2.20	2.44	2.41	±0.11	2.59	±0.11	4.25
		2.30	2.55					
	min = 255.41	2.20	2.28					
		2.30	2.39					
1500.00	max = 240.12	4.20	4.11	4.34	±0.47	0.66	±0.47	70.68
		5.00	4.90					
	min = 222.23	4.20	3.80					
		5.00	4.53					

2.5 Results and discussion

The results for the 5 cc/min injection case was compared with the experimental results as shown in Figs. 2.6 and 2.7. The dotted lines indicate the experimental results.

Even though the quality of the match for both flow rate and pressure drop are not quite good due to using a single fracture model, which assumed smooth fracture surface between two parallel plates but the simulation results follows the trend of the laboratory results.

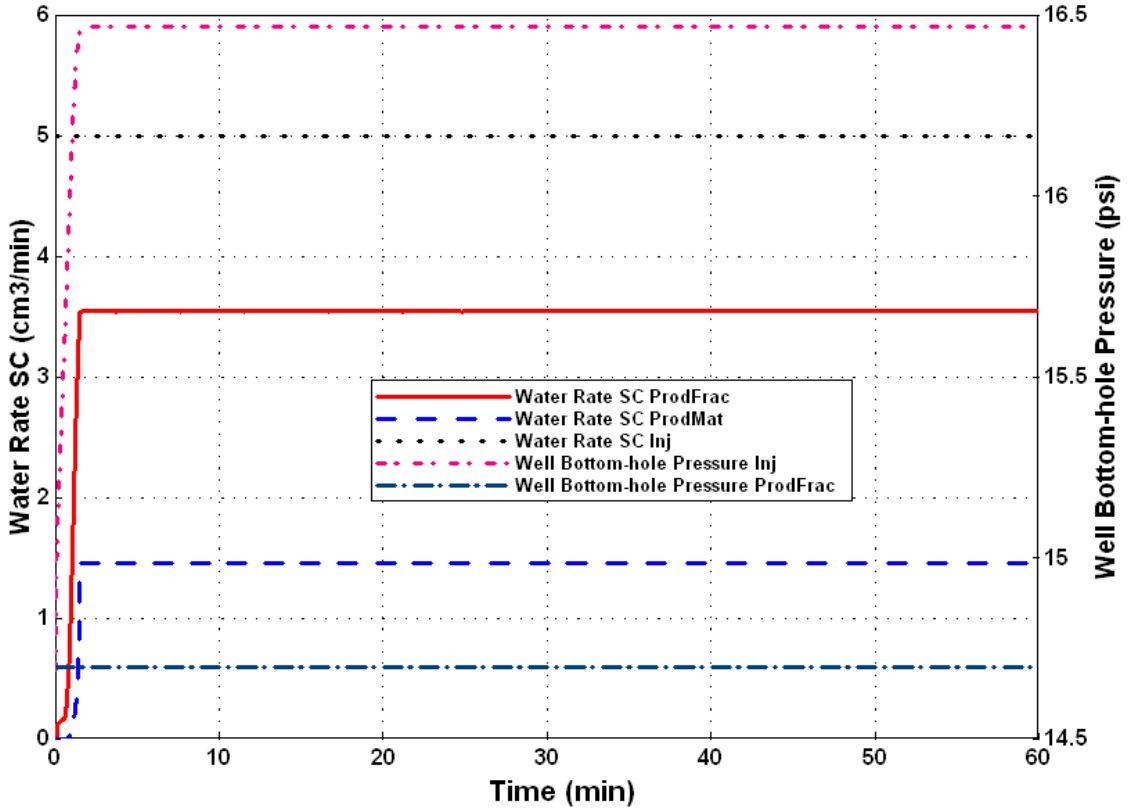

Figure 2.5 – The simulation results of flow rates and pressure drop injected at 5 cc/min and overburden pressure of 500 psi.

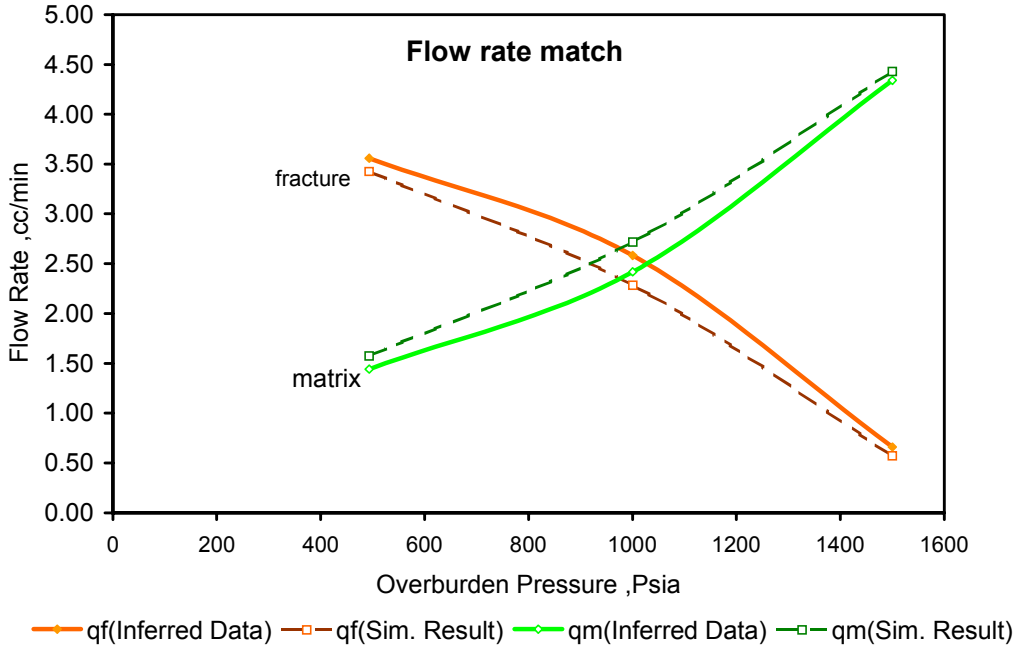

Figure 2.6 – The average flow rate comparison between laboratory and simulation results at 5 cc/min and each different overburden pressure.

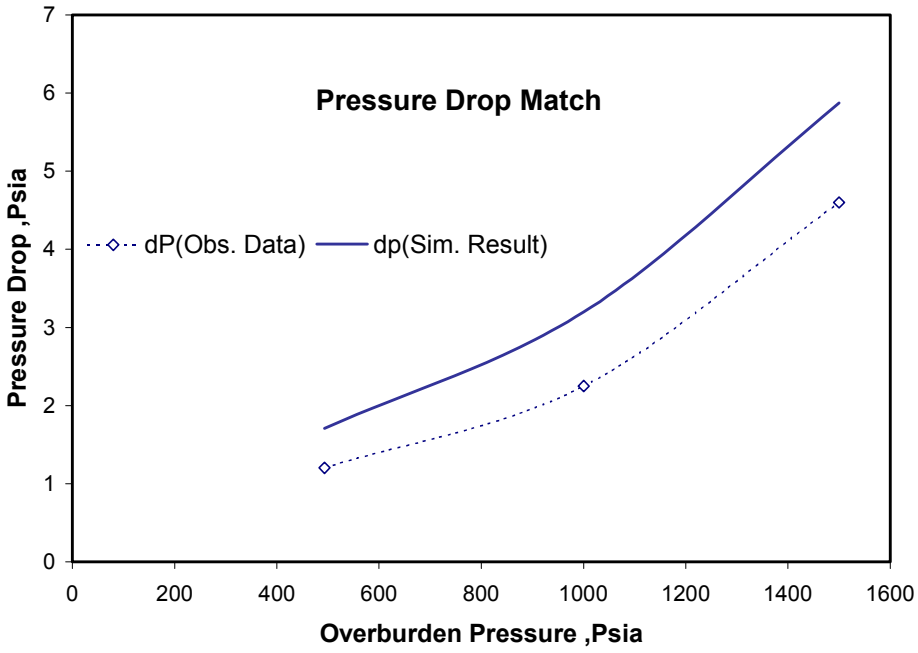

Figure 2.7 – The average pressure drop comparison between laboratory and simulation results at 5 cc/min and each different overburden pressure.

To make sure that resulting discrepancies in flow rates did not arise due to assumption or the error involved in the experimental measurement, modeling was done to match the experimental observation, namely the pressure drop across the core. Figures 2.8 and 2.9 show the matching between experimental and simulated results for average pressure drop across the core and flow rates, respectively. The aperture widths and their corresponding permeabilities with overburden pressures for the pressure drop match are given in Table 2.4. From the resulting average fracture flow rates, the effective aperture width was back-calculated from (5). The results of the effective aperture width calculated from fracture flow rates and the comparison to the effective aperture widths inferred from experiments is given in Table 2.5. The results reveal that the effective fracture aperture widths obtained by matching the average pressure drop (actual measured parameter in the experiments) is outside the range of effective aperture widths inferred from experiments. So the deviations from the cubic law did not arise due to the assumption or the error involved but could be due to the rough nature of the fracture surface. Even if we assume that the deviation in flow rates was due to the error involved, a simultaneous match for the average pressure drop and the average flow rates could not be achieved.

Table 2.4- Fracture properties obtained from pressure drop match.

Overburden Pressure (psia)	Fracture aperture (microns)	Average Kf (md) dp match
498.05	74.5	470,000.00
985.65	57.6	280,000.00
1500.5	41.3	146,500.00

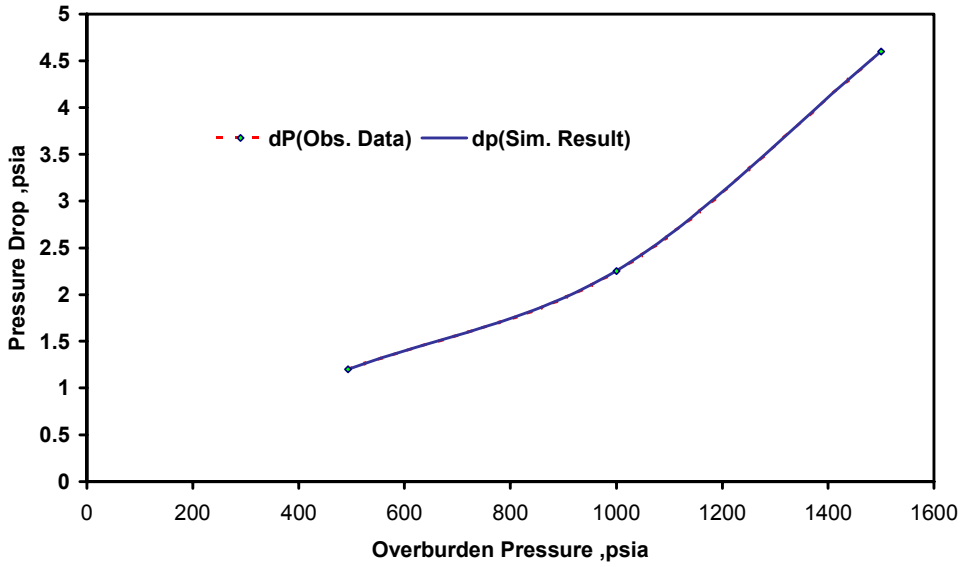

Figure 2.8 – The average pressure drop match between observed and simulation results for the fractured core experiment for 5 cc/min injection rate.

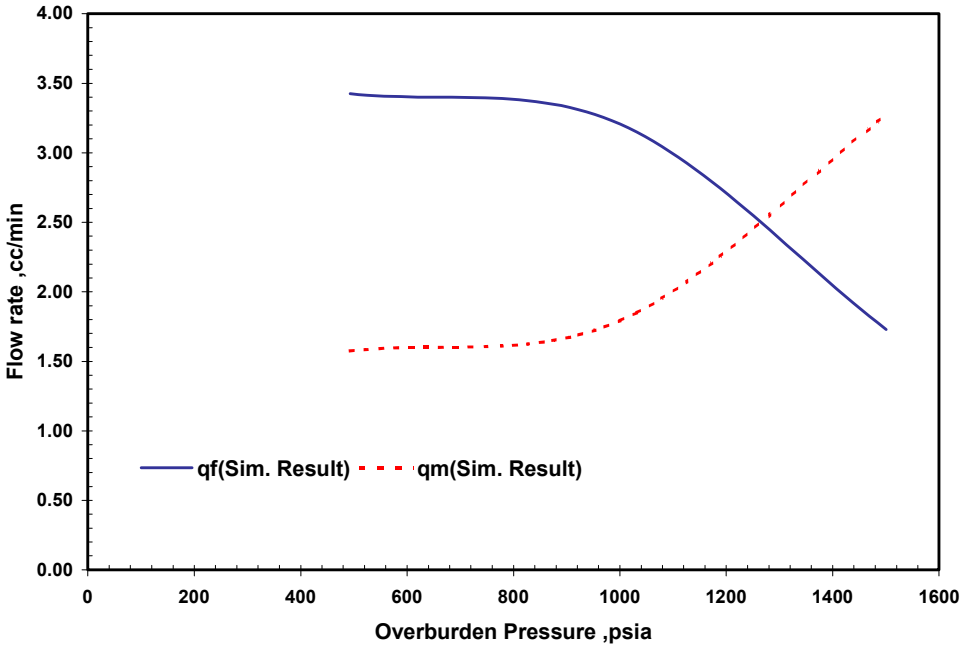

Figure 2.9 – The average flow rates observed for the corresponding average pressure drop match across the core at 5 cc/min injection rate.

Table 2.5- Comparison of fracture properties from simulation and experimental results.

Qinj	Pressure	Aperture width(experiments)		Aperture width(simulation)
cc/min	psia	mean (microns)	σ (microns)	microns
5	500	56.15	±4.73	74.51
	1000	40.40	±0.59	54.62
	1500	20.57	±5.80	41.36

The fracture aperture and fracture permeability are usually considered to remain the same during the producing life of the reservoir regardless of degree of depletion. Our experimental results show that the fracture aperture and fracture permeability have significant pressure-dependent changes in response to applying variable injection rates and overburden pressures. This is illustrated in Figures 2.10 to 2.12, which show the effect of several injection rates on matrix permeability, fracture aperture and fracture permeability, respectively, under variable overburden pressures. The effect of several injections on matrix permeability is not significant in contrast with that effect on fracture aperture and fracture permeability. During constant injection rates of 5 to 20 cc/min, the average matrix permeability decreases about 24% at overburden pressure of 1500 psia from its original value at 500 psia. Meanwhile, the effective fracture aperture width and fracture permeability decrease about 64% and 88%, respectively, from its original value.

Studying the effect of injection rates at different overburden pressures (Fig. 2.11) reveal an interesting phenomenon. After the first injection rate at 500 psia, the fracture aperture at injection rates of 10, 15 and 20 cc/min has similar values. Meanwhile at high overburden pressures, the effect of injection rates on fracture aperture is more obvious. As the overburden pressure increases, high rates of injection reduce the equivalent fracture aperture width. The fracture aperture becomes smaller at higher injection rates, which is *opposite* to the common thought. The reason behind this phenomenon is because the core has high matrix permeability and surrounded by constant high confining pressure that does not allow core to expand.

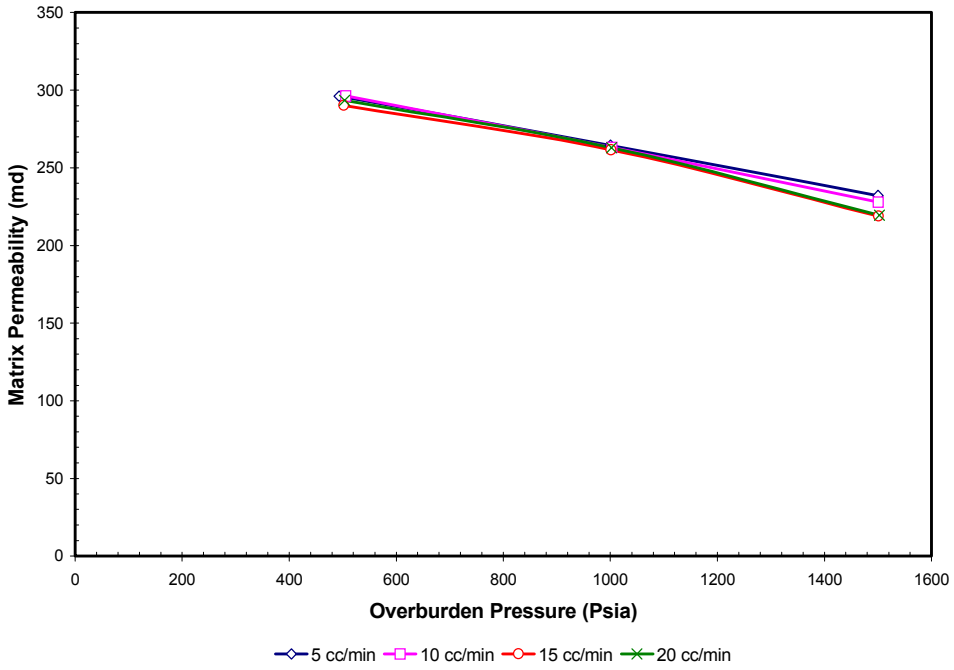

Figure 2.10 –Effect of injection rates on matrix permeability with varying overburden pressures.

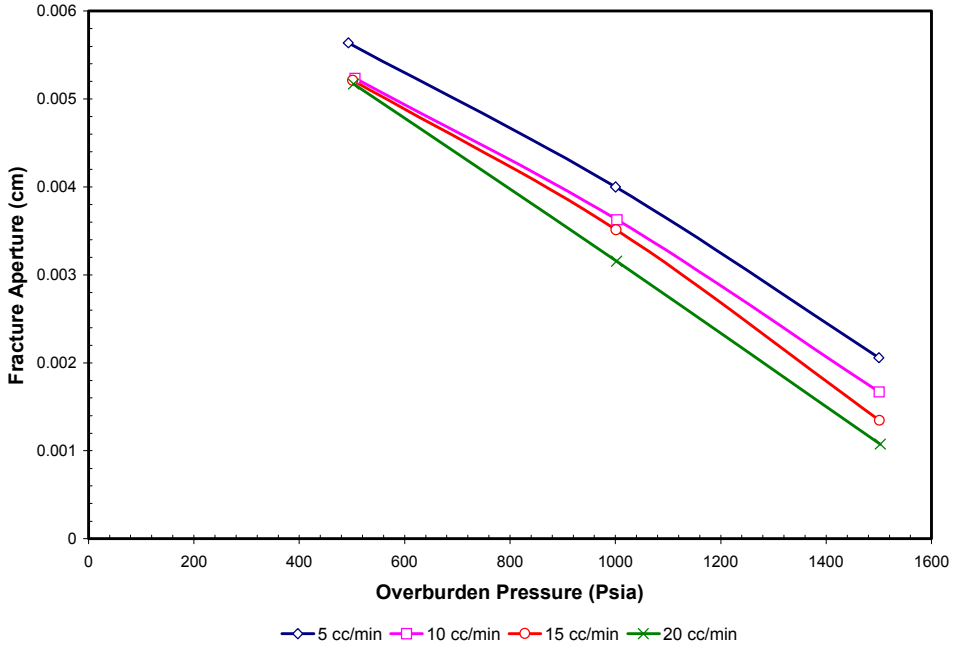

Figure 2.11 – Effect of injection rates on fracture aperture with varying overburden pressures.

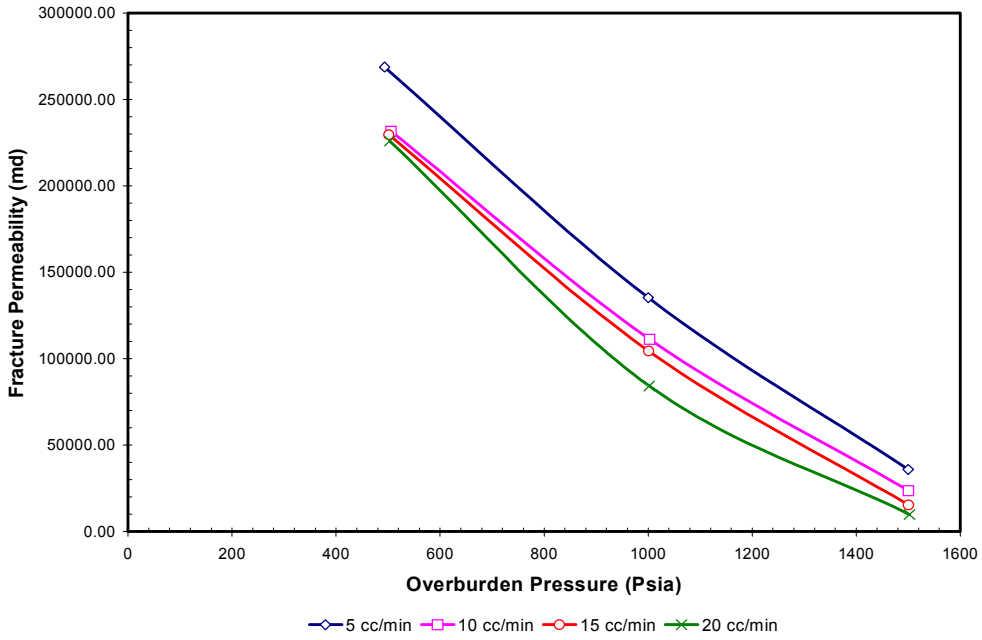

Figure 2.12 –Effect of injection rates on fracture permeability with varying overburden pressures.

Also the amount of flow through the fracture at different injection rates drops dramatically and they almost flow at similar rate at confining pressure of 1500 psia (about 1 cc/min) as shown in Fig. 2.13. It means that the water mostly flows through the matrix diverting from the fracture path. At higher injection rates, the pressure drop becomes higher through the matrix and increases tendency to squeeze the fracture aperture. That is why the fracture aperture becomes smaller at higher injection rates.

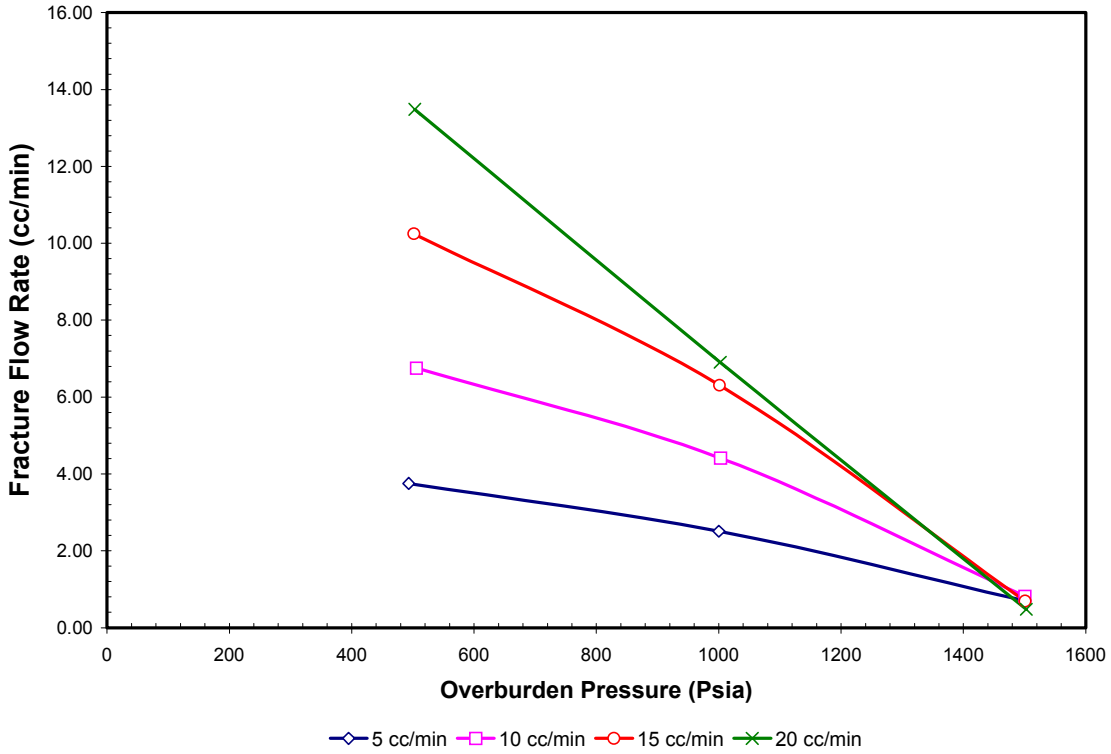

Figure 2.13 – Reduction in fracture flow rate with increasing overburden pressures.

The results also indicate that the influence of high stress on axial direction by introducing high injection rates would give high permeability reduction as also previous reported by Gray *et al.* [21] Because the fracture width is a function of fracture permeability, thus, the fracture permeability has similar trend as fracture width under different overburden pressures. The fracture permeability ranges from about 200-700 darcys at 500 psia reduces to about 9-36 darcys at 1500 psia.

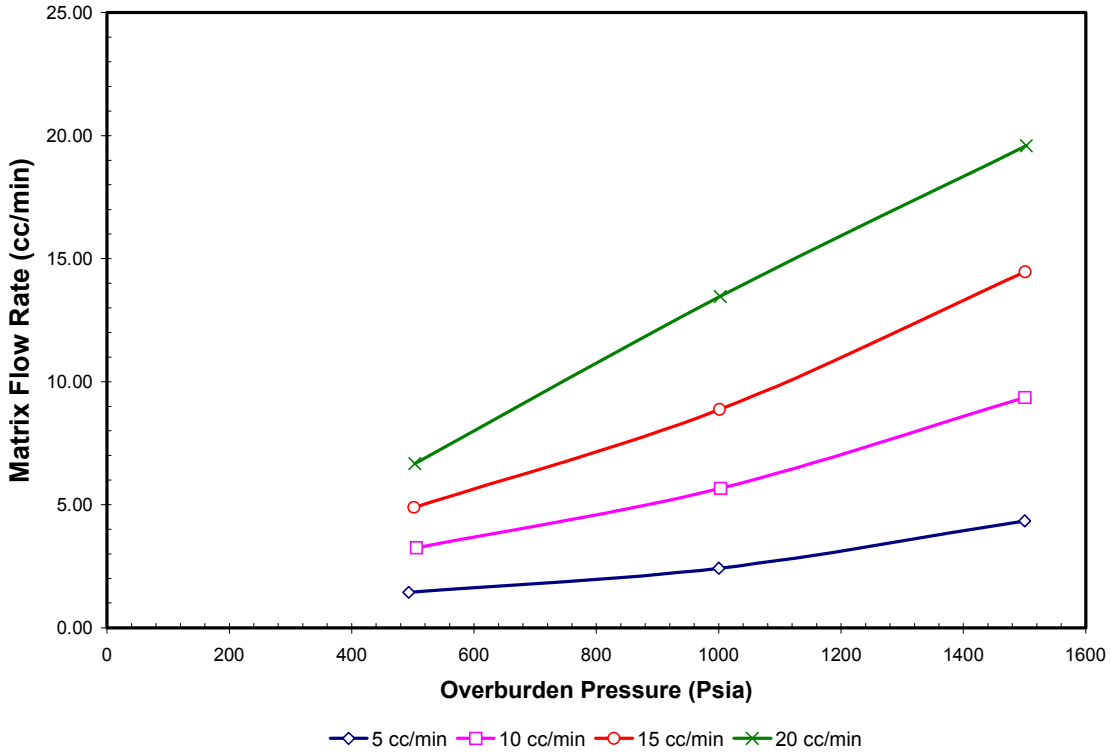

Figure 2.14 – Increase in matrix flow rate with increasing overburden pressures.

The effect of reduction fracture permeability clearly has significant effect on reservoir productivity. Thus, we determine how much the reduction of fluid flow through the fracture because of reduction in fracture permeability. It is also important to quantify of the flow through the matrix and the fracture at different overburden pressures. By applying Equations 4 and 5, we were able to quantify the contribution of fluid flow from matrix and fracture as shown in Figs. 2.13 and 2.14 at variable overburden pressures. At 500 psia, the flow is preference to the high permeability zone. In this time, the percentage range of fluid flows through the fracture at injection range of 5 to 20 cc/min is 72% to 68%. Meanwhile, after increasing the overburden pressure the fluid flow through the fracture decreases. At 1500 psia, the percentage range of fluid flow through the fracture at different injection rates is only about 14% to 2%. At this time most of injected water diverts through the matrix because of significant reduction of permeability in the fracture. Even though the fracture permeability is still very high (10 to 40 darcys) the volumetric

rate of flow through fracture decreases, therefore, most of the water flows through the matrix rock having less permeability (>200 md) but higher volumetric rate.

2.6 X-ray CT scan results

In an attempt to study the movement of brine in a fractured core, a simple experiment was carried out using an X-ray CT scanner. The experiment process involved injecting water at a rate of 0.5 cc/min from the top-centre of the core. The injection was done through the fracture. The movement of brine on a cross section perpendicular to the fracture observed through the CT-Scan is presented in Fig. 2.15.

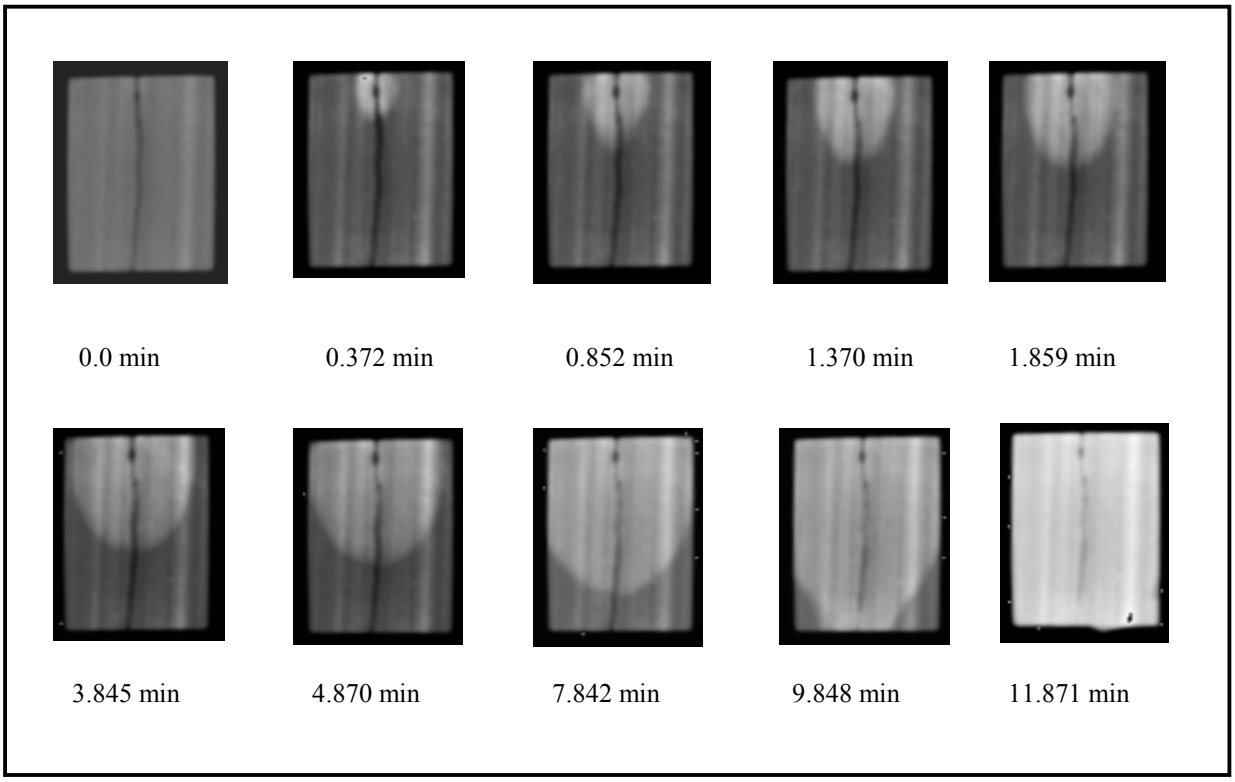

Figure 2.15– X-ray CT scans (perpendicular to the fracture) of single-phase gravity drainage experiment through a fractured core.

The experiment was modeled using a commercial simulator. The fracture was modeled as smooth plates hence having a constant permeability layer. Since the aperture

value could not established through the scan pictures due to the resolution, an aperture value of 50 microns was assumed. From the observations, it was found that smooth fracture assumption failed to recreate the saturation-front movement seen through CT-scans (Fig 2.16). The fluid moved through the fracture quickly because of its high permeability.

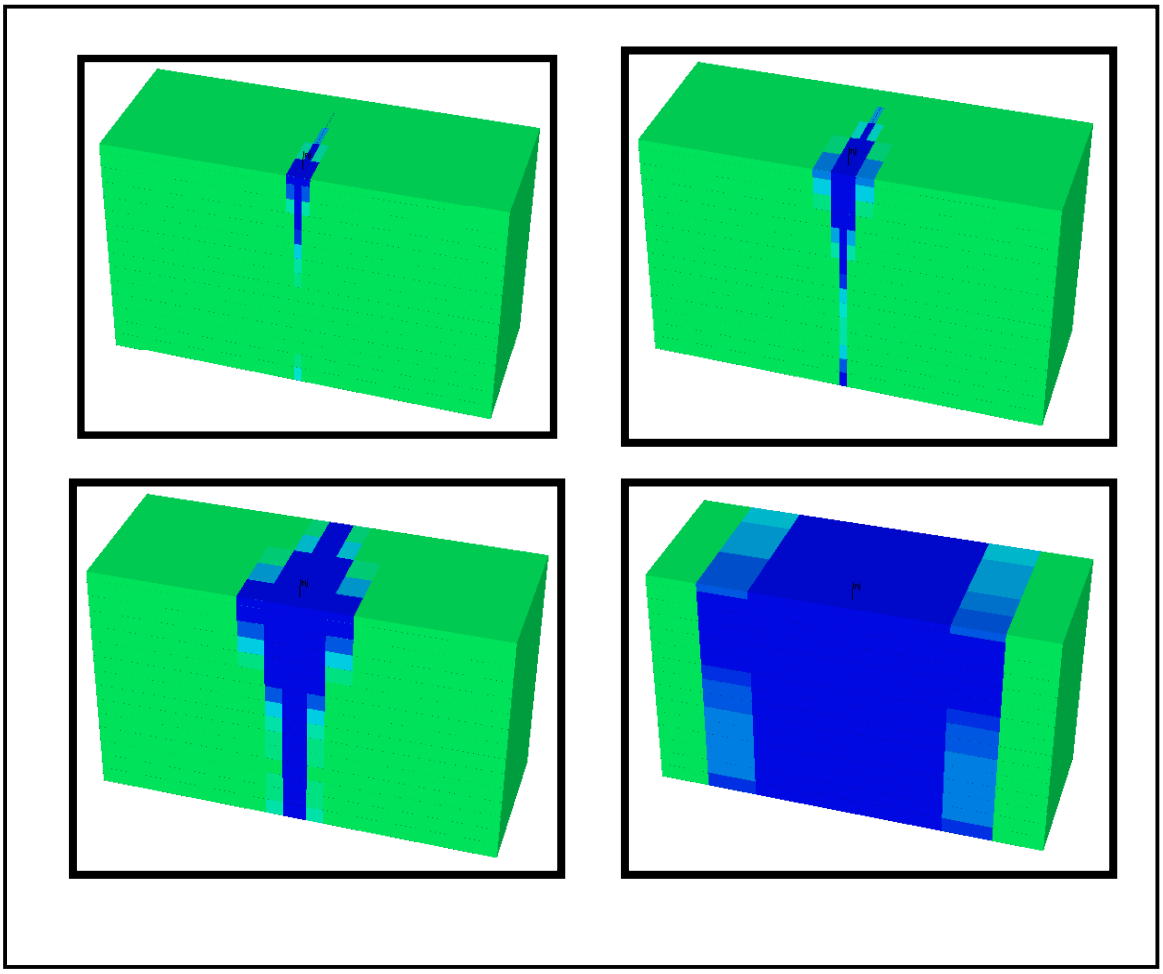

Figure 2.16 – Fluid movement through a core with smooth fracture.

Hence for modeling purposes a parallel plate approach for fractures fails to portray the true nature of flow. The flow on smooth fracture surface is found to be different than flow on rough fracture surface. As we could see from scans and modeling

results, the shape of sweep occurring in a plane perpendicular to the fracture is not adequately described by parallel plate modeling. Hence there is a need to model fractures quite different from what has been done in the past.

2.7 Conclusions

1. The change in matrix permeability with different injection rates under variable overburden pressures is not significant in contrast with that effect on fracture aperture and fracture permeability.
2. The experimental results of a core-induced fracture with high permeability matrix reveal that higher injection rates give smaller fracture aperture at constant high confining pressure.
3. The simulation results suggest that a parallel plate model is insufficient to predict fluid flow in the fracture system. Consequently, the spatial heterogeneity in the fracture aperture must be included in the modeling of fluid flow through fracture system.
4. The results also infer that the effect of stresses may be most pronounced in fractured reservoirs where large pressure changes can cause significant changes in fracture aperture and related changes in fracture permeability.
5. At high overburden pressure the influence of existing fracture permeability is not too significant. This conclusion is limited to the berea core which has high matrix permeability.
6. X-ray CT scans reveal that parallel-plate modeling of fractures seldom reflect the true nature of flow through fractures.
7. The laboratory result shows that the change in overburden pressure significantly affects the reservoir properties such as fracture aperture and fracture permeability.

CHAPTER III
GENERATION OF TWO-DIMENSIONAL FRACTURE APERTURE NETWORK THROUGH GEOSTATSISTICS

3.1 Fracture aperture measurement – introduction and background

Fracture aperture is the key parameter in determining the flow and transport characteristics of fractured media. In natural fractures there is usually a large distribution of fracture apertures even within a single fracture. The fracture aperture distribution is controlled by a number of factors, among them the flaws and inclusions in the material and the history of mechanical, thermal and chemical stresses on the material, from before it fractured, through the primary fracturing process and the subsequent fracturing episodes on to its current state.[24,25] A sudden release of the confining pressure may result in a widening of the fractures. Fracture spacing, which may be a result of both material strength and stress history, also affects the fracture aperture distribution.

Prediction of the fracture aperture distribution given the material properties and stress history (even if it could be somehow precisely determined over millions of years) is next to impossible, since the material is likely to fail at flaws or inclusions in the matrix, which cannot be captured in the averaged material properties. Field determination of the fracture aperture distribution, or even simply mean aperture, is currently an area of active research. Several direct techniques for detecting and imaging fractures are under development. Small-scale features can be imaged using video imaging inside a well, [26,27] which of course only provides an image of the fracture aperture in the immediate vicinity of the well, where the aperture of the fractures is most likely affected by the well boring process. For larger scales, geophysical imaging techniques include (1) seismic reflection, where seismic waves are generated at one location and measured at several points for 3D imaging, measuring the reflection of the seismic energy at discontinuities; (2) electrical methods, which rely on the fact that water-filled fractures have a higher conductivity than unfractured rock and can mobilize ions in solution; and (3) ground-penetrating radar, in which electromagnetic radiation is applied in a similar manner as with seismic imaging but at much higher frequencies (10 to 1000 MHz), with propagation of the radar signal

depending on the dielectric constant and electrical conductivity of the materials and reflection of the signal at discontinuities. At present, these geophysical imaging methods are successful only in detecting only very large features, with resolution at best of the same order as the dominant wavelength of the input signal for radar and seismic imaging (0.1 to 10's of meters), and 1 to 10 m for electric profiling. [28]

Indirect techniques of measuring the statistics of the fracture aperture distribution (arithmetic mean, geometric mean and standard deviation) include pumping and tracer injection tests. These are currently the most accurate means of assessing fracture aperture and its distribution in the field. At the laboratory scale, much higher resolution can be attained in the determination of the fracture aperture distribution. The higher resolution can be used to increase our understanding of the controlling mechanisms and key parameters for flow and transport in fractured porous media.

Several techniques have been applied to determine fracture aperture in the laboratory. The two surfaces of an open fracture can be scanned using a surface profiler, [29,30] providing a map of the surface roughness at a theoretical resolution of 10 μm for surface features. The two halves are then closed using a precise guidance mechanism. The fracture aperture distribution is computed indirectly by knowing the distance between the two halves. Although this technique can in principle be very precise, there is a high probability that the confining pressure may change during a flow experiment, or that the referencing between the two halves may not be adequate, resulting in an error in the estimated fracture aperture distribution. In addition, the surface profiling process may affect the surface due to the direct application of mechanical force.

The fracture aperture distribution can also be determined by injecting a fluid into the fracture that can be solidified, such as resins[31] or low melting point metals.[32] These methods may yield the desired aperture information, but render the fracture useless for flow experiments. Non-intrusive methods of determining the in-situ fracture aperture, within a core holder, at a given confining pressure, are thus more desirable. This would call for the use of computer-aided Tomography or X-Ray CT scan. This would lead to very high processing costs, which only a few companies could afford. Therefore

alternative methods for finding fracture aperture width and the fracture distribution have to be sought.

3.1.1 Stochastic generation of aperture network

As an alternative to deterministic models, some investigators have used stochastic methods of characterizing fracture occurrence and flow in fractures. Given a sufficient data set and an appropriate distribution, the statistical moments of fracture occurrence, orientation, spacing, and aperture can be described. From these values, equivalent statistical models of fracture fields can be generated. Shimo and Long[33]have generated stochastic fracture fields by working from several different conceptual models.

Brown and Scholz[30] used several aperture-averaging formulas, including arithmetic average aperture, in the cubic law to approximate the fluid flow in his numerically simulated fractures with isotropic random aperture fields. He determined that the flow calculated from the cubic law using the arithmetic average aperture, instead of the other aperture averaging formulas, better approximated the flow from his numerical simulations.

In this research geostatistical methods were used to generate a fracture distribution and then perform flow experiments through them and attempt to match the experimental results. An aperture density distribution is employed to represent the range of aperture values in a single fracture. The aperture values of laboratory core samples usually follow a skewed distribution well approximated by a log-normal distribution.[29-31]

3.1.2 Log – normal distribution [34]

The log normal distribution is closely related to the normal distribution. If the logarithm of a variable is normally distributed, then the variable itself is log normally distributed. The log-normal distribution is skewed with a long tail on the right hand side. However, after transforming the data by taking the log of the variable, the distribution becomes symmetric and normal. If we consider X to be a log normally distributed variable, then we can define Y= ln X, where Y is the value of the natural logarithm of the random variable X. If the mean of the variable Y is α and the variance is β^2, we can write the probability density function for the variable X as,

$$f(x) = \frac{1}{x\beta\sqrt{2\Pi}} \exp\left[-\frac{1}{2}\left(\frac{\ln x - \alpha}{\beta} \right)^2 \right] \tag{6}$$

The mean and variance of the random variable X, is related to the mean and variance of the transformed variable Y through,

$$\alpha = \ln \mu - \frac{\beta^2}{2} \tag{7}$$

$$\beta^2 = \ln\left[1 + \frac{\sigma^2}{\mu^2} \right] \tag{8}$$

where μ is the mean of the variable X, and σ^2 is the variance of the variable X. So given a mean and variance of a variable, we can generate the log-normal values by first deriving the mean and variance from equations 7 and 8, and then standardizing this using,

$$z = \frac{\ln x - \alpha}{\beta} \tag{9}$$

This is similar to the normal distribution. So by choosing a range of values for z , we can generate a range of values for x. Figure 3.1 illustrates an example of log normal distribution with a mean of μ=56.4 and different variances σ^2.

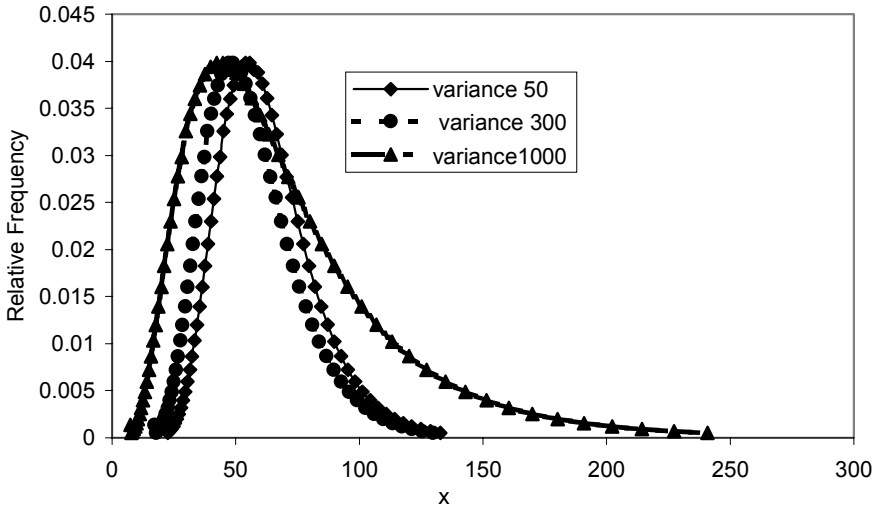

Figure 3.1 – Illustration of log normal distributions with a mean of 56.4 and different variances.

It was mentioned earlier that aperture values obey a log normal distribution, which is characterized by two parameters: the mean aperture and the standard deviation. Since actual sample values of apertures are not available for this research, the log-normal distribution function is utilized to create sample values of apertures. These sample values of apertures may not be enough to define a more approximate fracture surface. Therefore more values are sought.

Initially all the aperture values were obtained from the lognormal distribution, but the resulting aperture distribution *did not successfully* match the experimental results. Even though the modeling matched the flow rates, the pressure drop could not be matched simultaneously. This was similar to the case of parallel plate model shown earlier. The results of the simulation runs for the injection rate of 5 cc/min are shown in Figures 3.2 and 3.3.

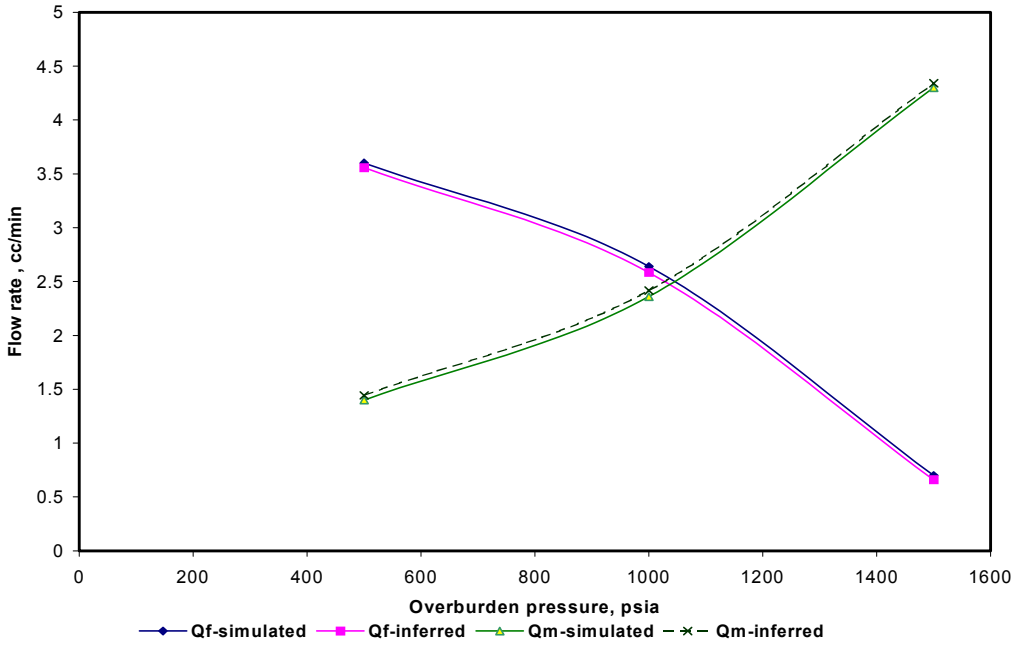

Figure 3.2 – Average flow rates match using apertures generated entirely from lognormal distribution for the 5 cc/min injection rate.

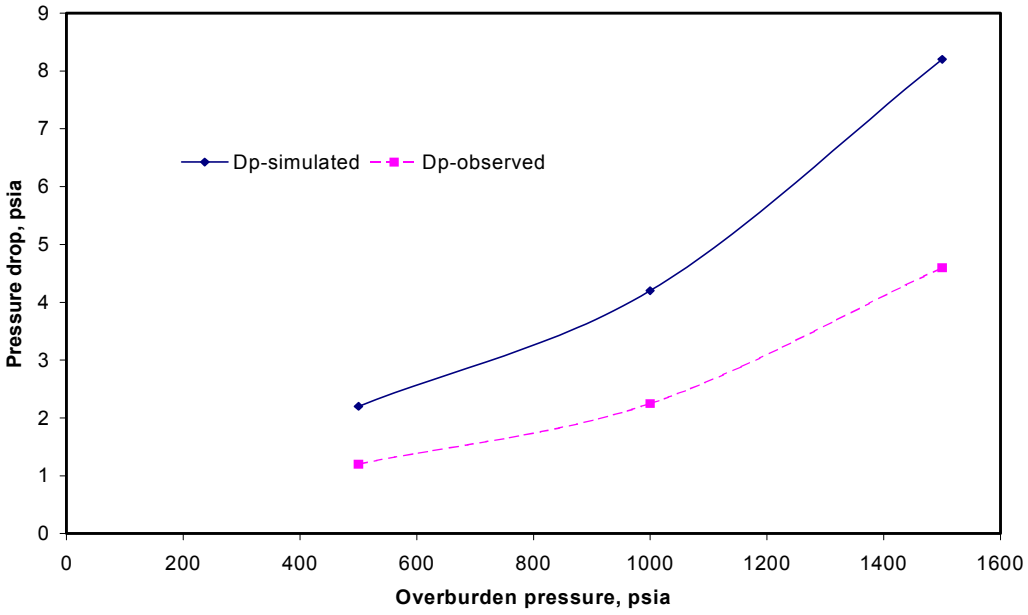

Figure 3.3 – Average pressure drop match using apertures generated entirely from lognormal distribution for the 5 cc/min injection rate.

So using values entirely off the lognormal distribution did not prove successful for the inferred experimental results. Hence the need to use kriging to obtain more aperture values which may or may not have correlation to each other. Usually the number of values corresponds to the size of the grid used in simulation. In this research, the number of aperture values corresponds to the grid size used in simulation discussed later.

3.2 Kriging

Kriging is based on the assumption that the parameter being interpolated can be treated as a regionalized variable. A regionalized variable is intermediate between a truly random variable and a completely deterministic variable in that it varies in a continuous manner from one location to the next and therefore points that are near each other have a certain degree of spatial correlation, but points that are widely separated are statistically independent.[34] Kriging is a set of linear regression routines which minimize estimation variance from a predefined covariance model. There are several types of kriging like simple kriging, ordinary kriging, universal kriging, zonal kriging and indicator kriging. For this research ordinary kriging[34] is employed.

3.2.1 Generation of fracture aperture map from kriging

The aim of geostatistical modeling is to recreate the rugosity observed on a fracture surface. The log-normal assumption helps to generate sample aperture values. Generating all the fracture aperture values using lognormal distribution did not match the experimental results through simulation. This may be attributed to the presence of small aperture values. By using the mean fracture aperture width (μ) obtained from experimental analysis, and assuming different variances (σ^2), fracture aperture samples were generated. This was achieved by varying the range of the normal variable z from –3 to +3. Since the values were not correlated to each other, kriging was directly employed to generate the aperture distribution through the variances assumed.

To obtain a good match between experimental and simulated results, a spherical model with pure nugget was used with variances of 180, 100 and 30 (micron^2) for the overburden pressures of 500, 1000 and 1500 psia, respectively. The values of the

variances were obtained through trial and error. Figures 3.4-3.6 show the fracture aperture distribution maps generated through kriging.

It is observed that, as the overburden pressure increases, the fracture surface becomes smoother. This may be attributed to the fact that as the overburden pressure increases, the asperities on the fracture surface are broken down and the surface tends to become smoother.

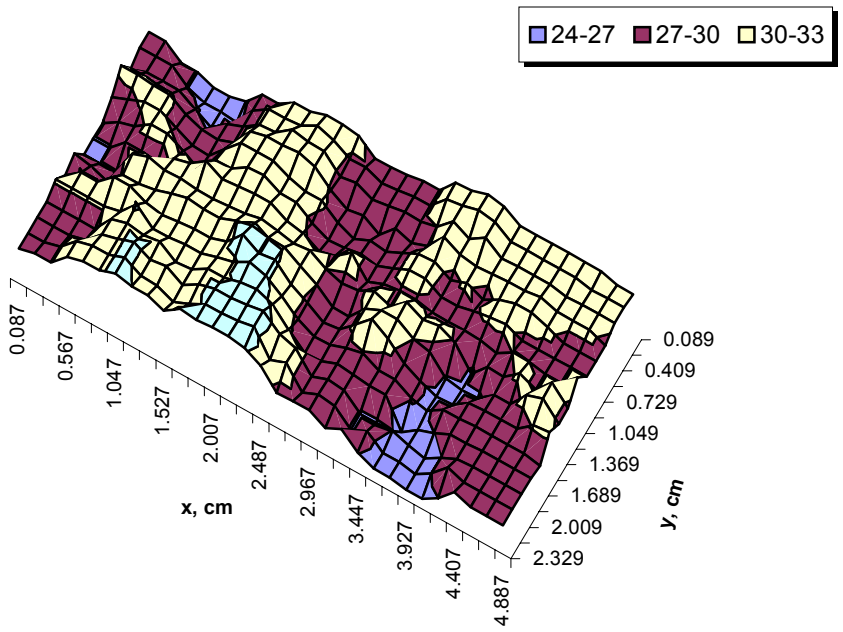

Figure 3.4– Kriged fracture aperture map for mean width = 56.4 μm and variance = 180 μm^2.

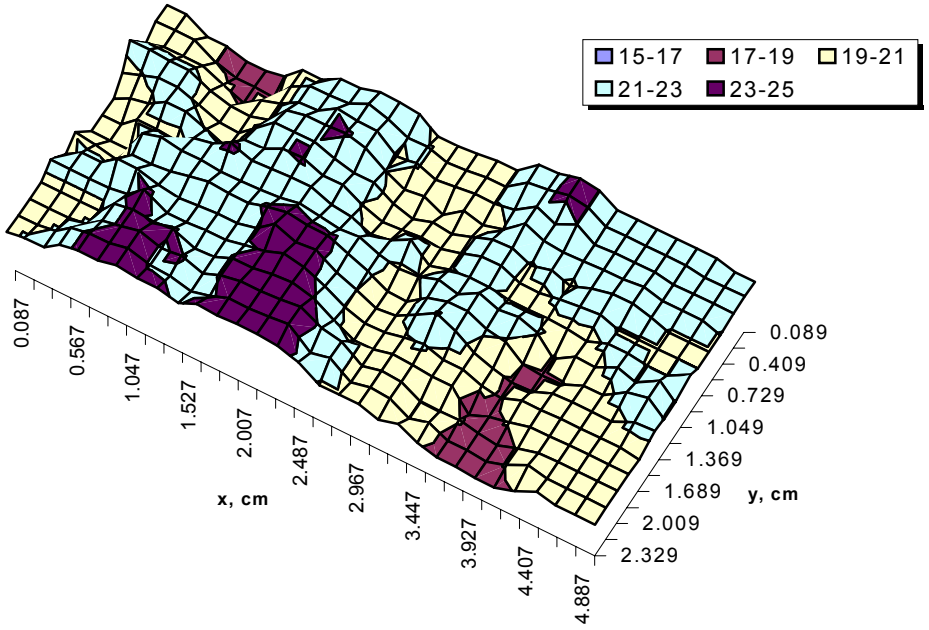

Figure 3.5 – Kriged fracture aperture map for mean width = 40 μm and variance = 100 μm^2.

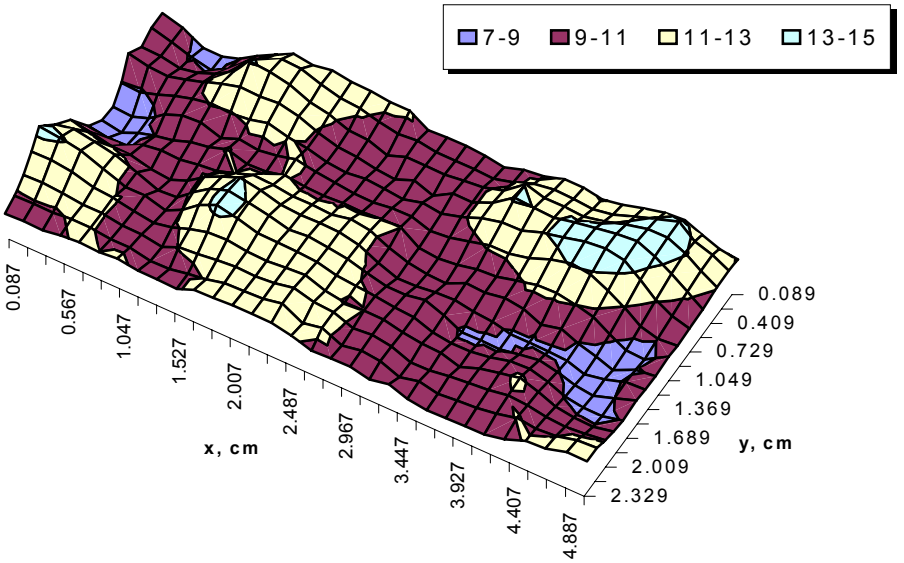

Figure 3.6 – Kriged fracture aperture map for mean width = 20 μm and variance = 30 μm^2.

3.3 Conclusions

1. Kriging is employed to generate a rough fracture surface since aperture values generated solely from lognormal distribution did not match the experimental observations.
2. In this research we have only chosen sample aperture values from a lognormal distribution as our initial guess. The resulting aperture values for the entire fracture surface did not correlate among each other.
3. This methodology of generating the apertures using a nugget effect can only be justified when compared to the actual aperture measurements using an X-ray CT scanner. But measuring the aperture values from X-ray CT scanner is beyond the scope of this thesis.
4. The fracture aperture system generated may not be a true representation of the actual fracture aperture network of the core surface. But it is very effective in producing an adequate match with the experimental observations.
5. The true aperture system though could only be measured with a high-resolution scanner. As for this research it is found med that the aperture values did not have a correlation among each other.

CHAPTER IV
NUMERICAL SIMULATION OF FLOW THROUGH SINGLE FRACTURES

4.1 Modeling fracture flow experiments

As pointed out earlier, modeling of flow experiments has posed a major challenge to the ongoing research on naturally fractured reservoirs. Tsang *et al*. [18] simulated similar flow experiments by generating a fracture aperture distribution and then with constant head boundary conditions on two opposite sides of the two-dimensional flow region, with closed boundaries on the remaining sides. The results show that the majority of flow tends to coalesce into certain preferred flow paths (channels), which offer least resistance. Tracer transport was also simulated using a particle tracking method. Tsang and Tsang [17] chose a statistical description of a fracture with variable apertures by means of three parameters, performed numerical flow and transport experiments with them with particular emphasis of correlate the fracture geometry parameters. But concluded that the correspondence between observations and the hydrological properties is still ambiguous.

None of the literature in the past points to a case where experimental results were matched with particular reference to "real" fracture surfaces and the effect of surface roughness in the form of "friction factor". Here we try to present such a case whereby laboratory data are analyzed and matched using a fracture aperture distribution and taking into consideration the effect of roughness on flow.

4.1.1 Simulation model

After having generated a fracture aperture map, we proceed to model the flow experiments. A numerical model utilizing commercial simulator (CMG™) was used to study the fluid flow through fractures at different overburden pressures. The laboratory process in which the water was injected through the fracture was duplicated in this modeling effort. The rectangular grid block (Fig.4.1) was applied to overcome the difficulty of modeling a cylindrical core shape.[2] Single porosity model was chosen since it was a discrete fracture running throughout the core in the middle. The volume of the core was maintained constant.

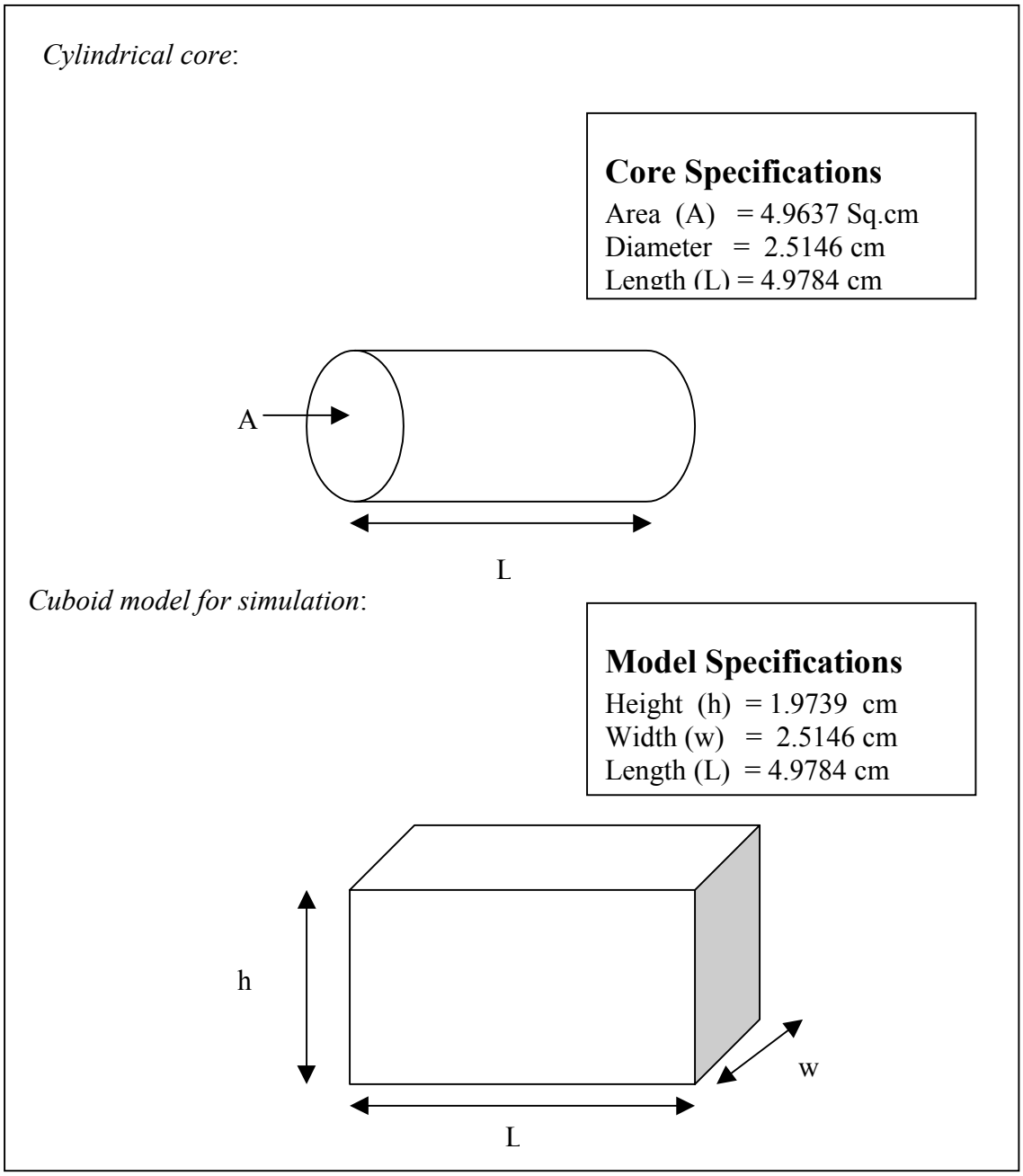

Figure 4.1 – Conversion from cylindrical model to cuboid model.

The first part of modeling any flow experiments is establishing the correct grid model that would enable the simulation of the experiments more accurately. From the experiments there are two sets of data, one from the matrix flow experiments (unfractured

core) and the other from fracture flow experiments (fractured core). In the first case flow experiments were conducted in an unfractured core and the data from these experiments was used to establish an appropriate model, which would be utilized to simulate the fractured rock experiments.

The model parameters (Table 3.1) are obtained after several simulation runs. The model was first tested for grid sensitivity. The sensitivity studies showed that 31*15*15 was an optimum grid sizing. The results were consistent with increased grid sizing in the X or Y direction. It is imperative to first determine if the model is correct and efficient. Matrix flow experiments (unfractured core) were simulated through the model to ensure the validity of the model. The results of the matrix flow experiments proved that the model we chose was good enough to simulate the flow experiments. Other model parameters were determined from the flow experimental data, from the properties of Berea core.

Table 3.1- Simulation model parameters.

Grid	31*15*15
Porosity	0.2358
Pore volume	5.827 cc
Density of water	1 g/cc
Compressibility	5.19295E-07 (1/psi)
Viscosity	1 cp
Reference pressure	7928.97 psia
Rock compressibility	4.35113E-07 (1/psi)

The simulation runs using the model gave impressive results. We were able to match the experimental observations for unfractured core experiments using the model. This ascertained the model we employed and allowed us to carry forward the model for fracture flow experiments. Figures 4.2-4.3 show the match (average pressure drop match) for the matrix flow experiments for various overburden pressures and flow rates of 5 cc/min and 10 cc/min.

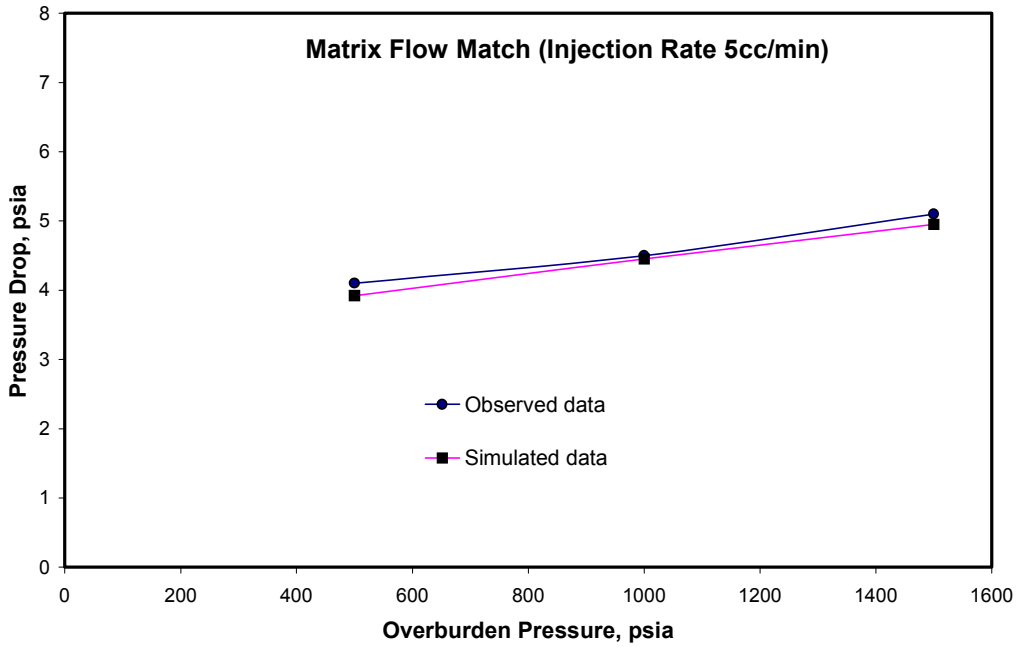

Figure 4.2 – History matching of matrix flow experimental data for Qinj= 5 cc/min.

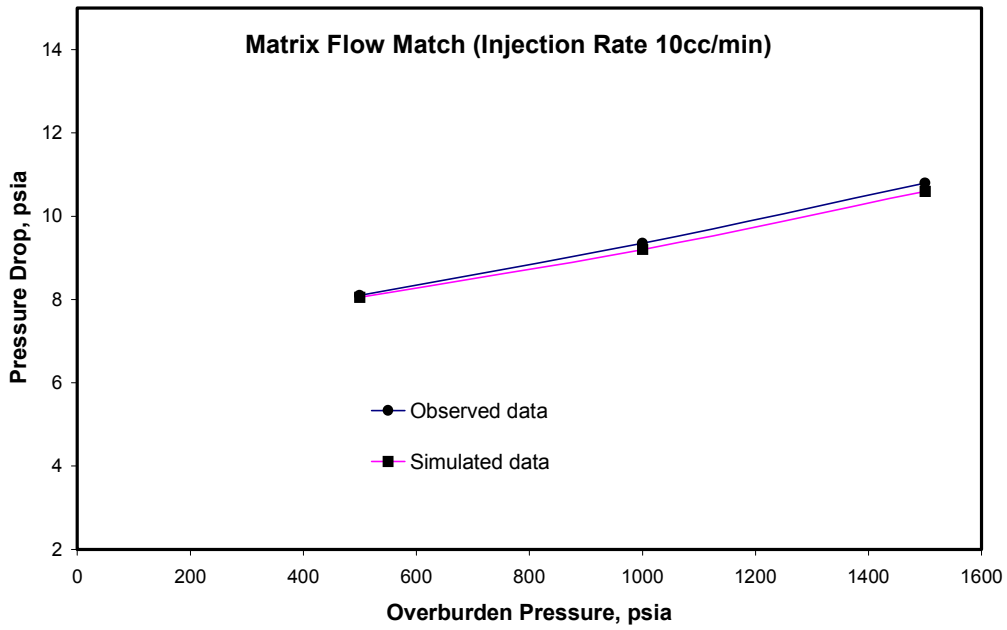

Figure 4.3 – History matching of matrix flow experimental data for Qinj= 10 cc/min.

4.2 Surface roughness implications on flow

The parallel plate model can be considered only a qualitative description of flow through real fractures. Real fracture surfaces are not smooth parallel plates, but are rough and contact each other at is discrete points. Fluid is expected to take a tortuous path when moving through a real fracture. Thus deviations from the cubic law are expected. The experimental work by Iwai[1] suggests that for rough-walled fractures under low normal stress, changes in the aperture result in changes in flow rate consistent with the cubic law. However, a 1-2 order magnitude error should result from neglecting the tortuosity when using the cubic law. This order of magnitude is obtained by simulating the flow electric current with resistors in its path.[13] In this research an attempt is made to explore and model the magnitude and nature of the disagreement between the parallel plate model and the actual flow through rough-walled fractures.

Several approaches have been used in the past that explicitly account for surface roughness. Various empirical flow laws have been presented that are based on

experiments with idealized geometry. One such experiment used parallel plates with sand glued to the walls to recreate small-scale roughness and another used parallel plates with various machining marks to recreate large-scale fractures.[1] There were many theoretical approaches that focused on redefining the cubic law to account for the surface roughness and the resulting tortuosity of the fluid flow paths.

4.2.1 Effect of friction due to local roughness

In order to effectively model the flow through fractures, we carefully observe the effect of surface roughness on flow. Since the surface of the fracture is rough, the roughness has to have an impact on the nature and magnitude of flow. Since the surface is rough the flow velocity is reduced because of the friction associated with it. Hence there is a decrease in flow rate when flow occurs through rough surfaces. In an experimental study of flow between sand-coated plates Lomize[7] found that the friction factor could be generalized through an empirical relation

$$f = 1 + 6\left(\frac{\varepsilon}{D_h}\right)^{1.5} \tag{10}$$

when $(\in/D_h) > 0.033$ and

$$f = 1 \tag{11}$$

when $(\in/D_h) < 0.033$

where the term $(\in/D_h)$ is known as the relative roughness, $\in$ is the absolute roughness and D_h is the hydraulic aperture(Fig. 4.4).

Louis(1969) through a similar experiment that flow could be made to fit the experimental data by introducing a friction factor,

$$f = 1 + 8.8\left(\frac{\varepsilon}{D_h}\right)^{1.5} \tag{12}$$

when $(\in/D_h) > 0.033$ and

$$f = 1 \tag{13}$$

when $(\in/D_h) < 0.033$

Both of these relations have been researched and found that both of them fit the data modeled by researchers in the past. For our purpose we have used Louis' empirical relation to fit our experimental data. The methodology will be discussed in the subsequent paragraphs.

In our research the relative roughness is calculated by taking ratio of the average roughness value over the hydraulic aperture of the fracture ($\in/D_h$), where $\in$ is the absolute roughness and D_h is the hydraulic diameter. Figure 4.4 illustrates the concept of relative roughness.

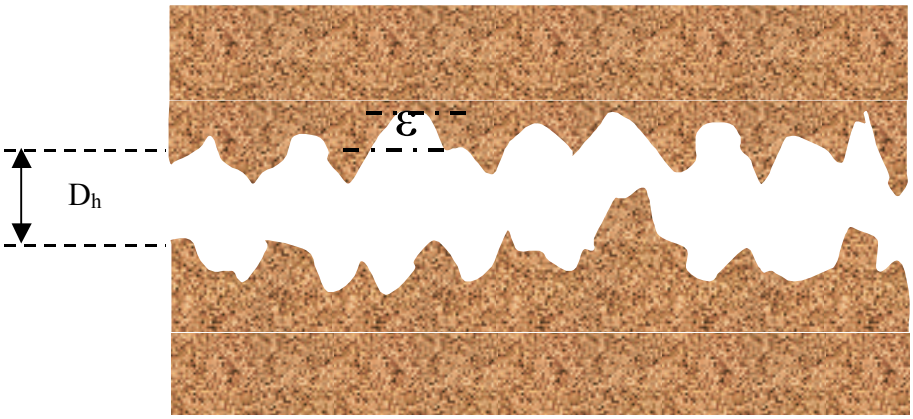

Relative Roughness: = ε/ D_h

Figure 4.4 – Relative roughness – An illustration.

4.2.2 Modification of permeability distribution

After generating the fracture aperture distribution, the effect of surface roughness is accounted for by modifying the permeability distribution in the fracture surface. The reduction in permeability due to local roughness is inferred through the following equation.

$$k_f = \left(\frac{1}{f}\right) 8.45\times10^{9}\, w^2 \qquad (14)$$

where, w is a fracture width in centimeters and f is the local friction factor calculated from the aperture distribution. Figures 4.5 and 4.6 show the difference in permeability distribution before accounting for roughness and after accounting for roughness. Modification of the permeability layer proved to be the key while simulating the fracture flow later to match the two parameters, flow rate and pressure drop across the core.

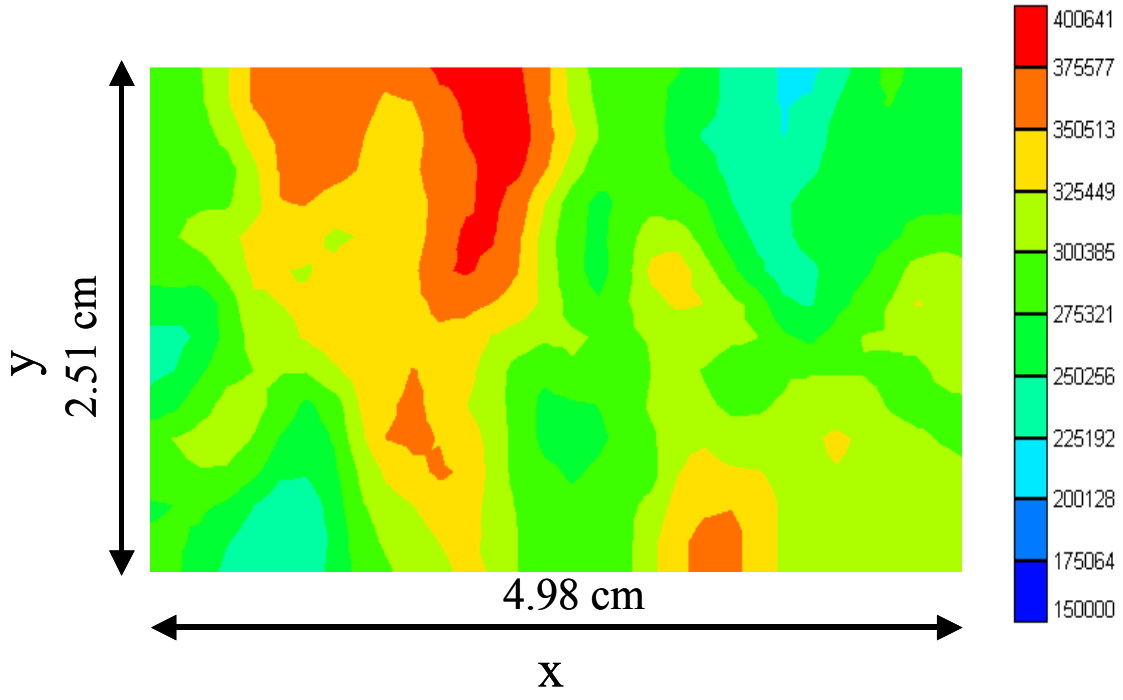

Figure 4.5 – Fracture permeability distribution before accounting for surface roughness.

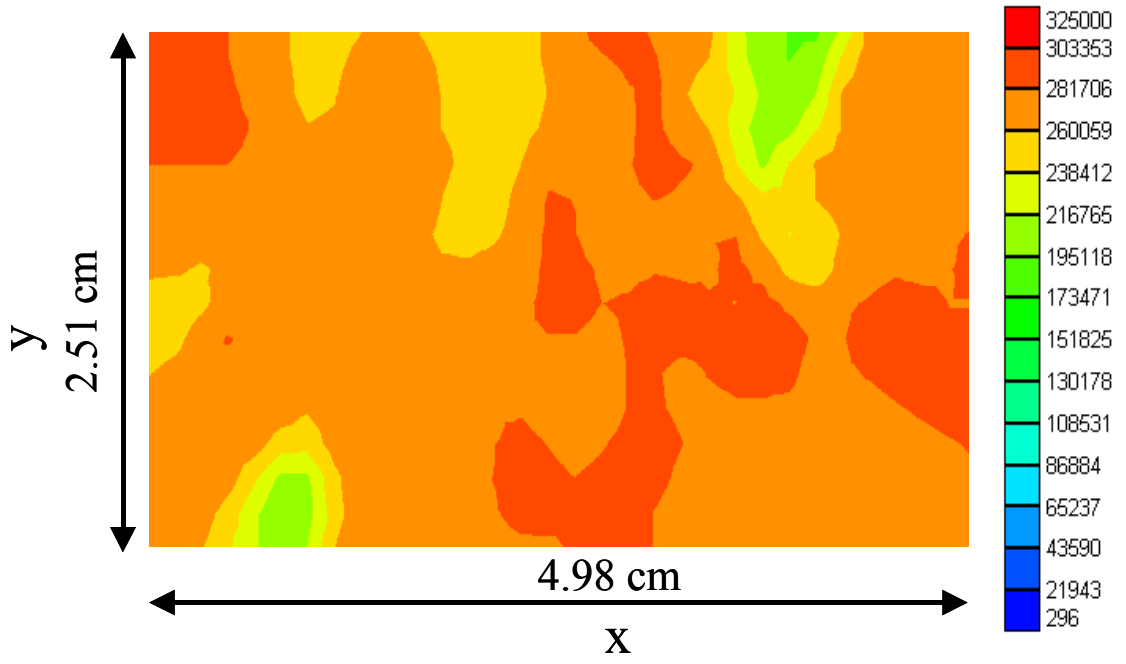

Figure 4.6 – Fracture permeability distribution after accounting for surface roughness.

The permeability map shown above (with friction case) was generated by locally applying (14). That is, the permeability of each grid block was calculated using (14). The resulting reduction in permeability can be visualized in Fig.4.7. As we can observe that the higher permeability values have been reduced and more values fall in the range of 227-263 darcies which correspond to an approximate effective aperture width range of 51-55 microns.

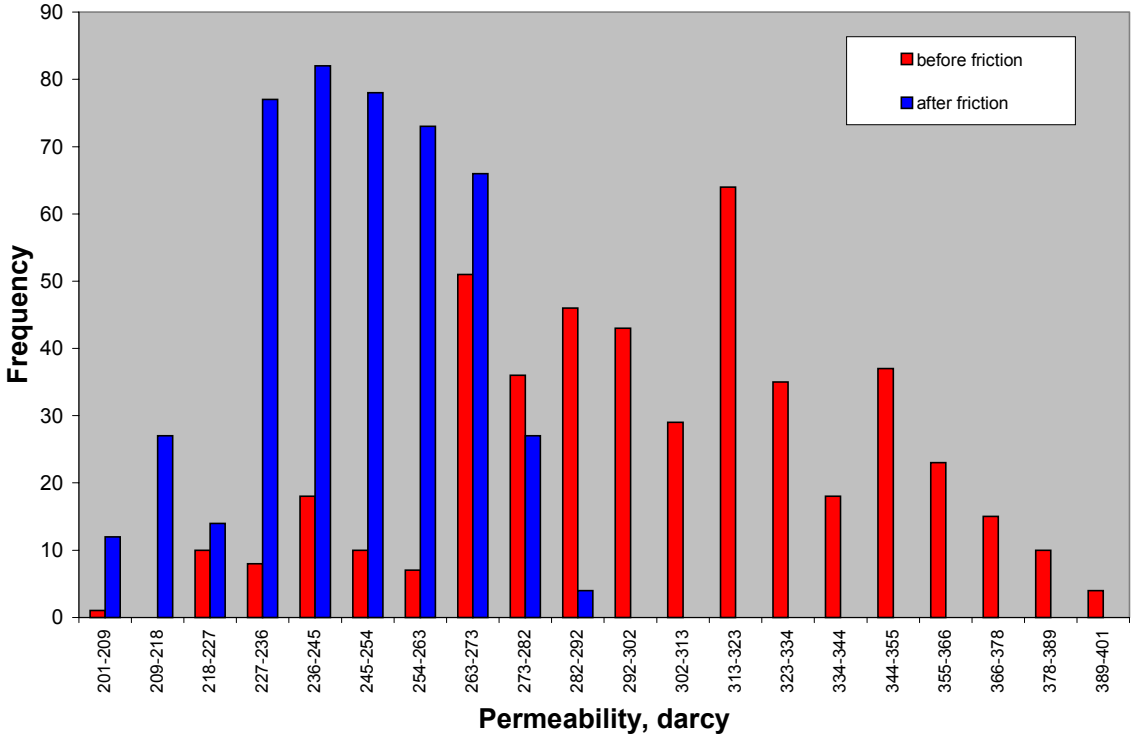

Figure 4.7 – Illustration of the reduction in permeability due to friction.

4.3 Fracture -flow modeling results

A 31x15 grid block sizing was used in the x and y directions with 15 layers in the z direction. The fracture layer was incorporated in the 8th layer and the rest are matrix layers. The modified permeability layer was used for the fracture layer, while the matrix layers had a constant permeability obtained from experimental analysis. For the first phase of preliminary results the simulation model was run for the 5 cc/min injection rate case. All the layers were injected with constant water injection of 5 cc/min through injection points located at one extreme end and penetrating through all the layers. At the opposite end two production points were located, one for the matrix layers and the other for the fracture layer, quantify the amount of water produced at those two points.

By introducing the corresponding modified permeability layer for the fracture, the results obtained were quite impressive. The results matched very closely, opening the door to more ventures through this kind of modeling. Earlier it was shown that by using a parallel plate model the simultaneous match was not possible i.e. though one could individually match flow rate by increasing the permeability, the pressure drop could not be matched simultaneously.

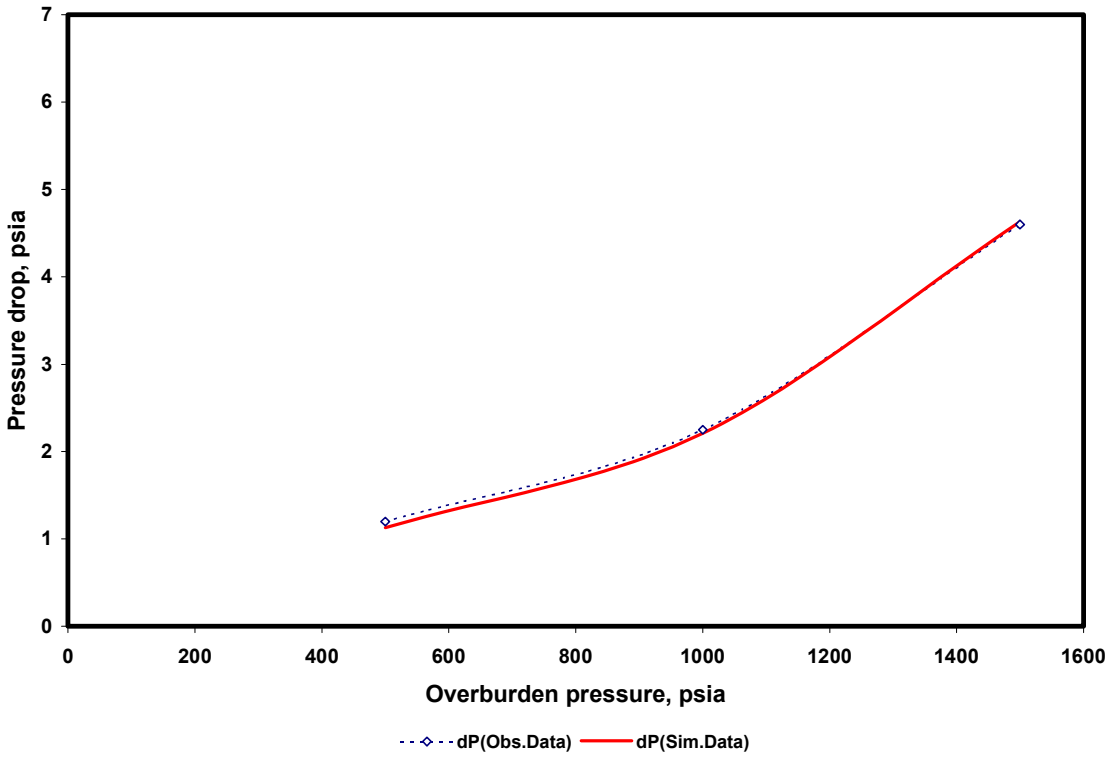

Figure 4.8 – Pressure drop match between experimental data and simulated data.

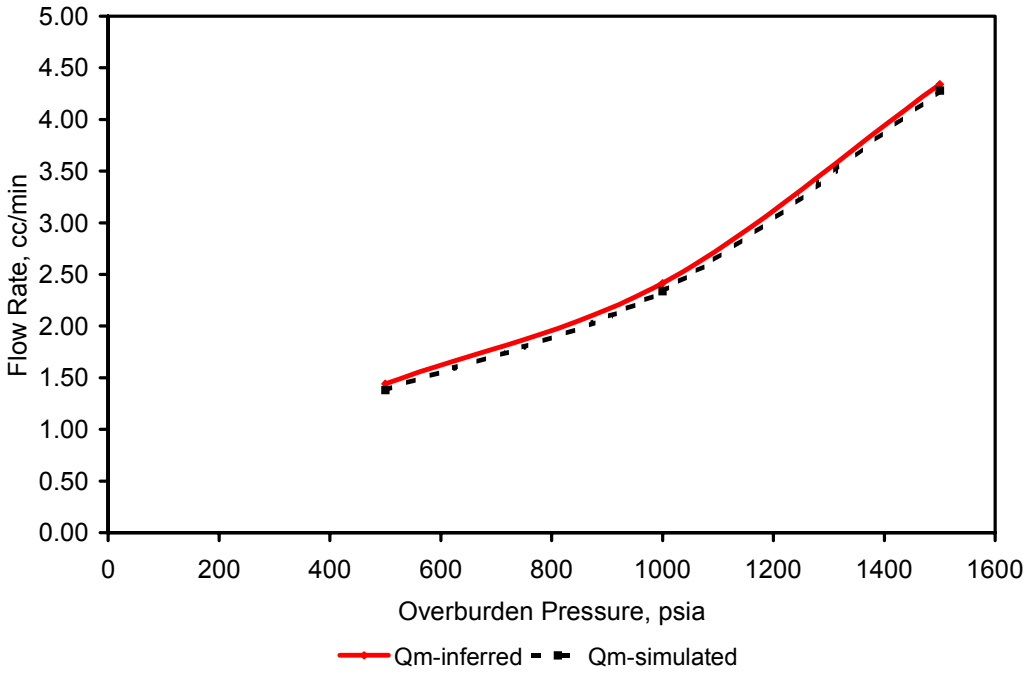

Figure 4.9 – Average matrix flow rate match between experimental data and simulated data.

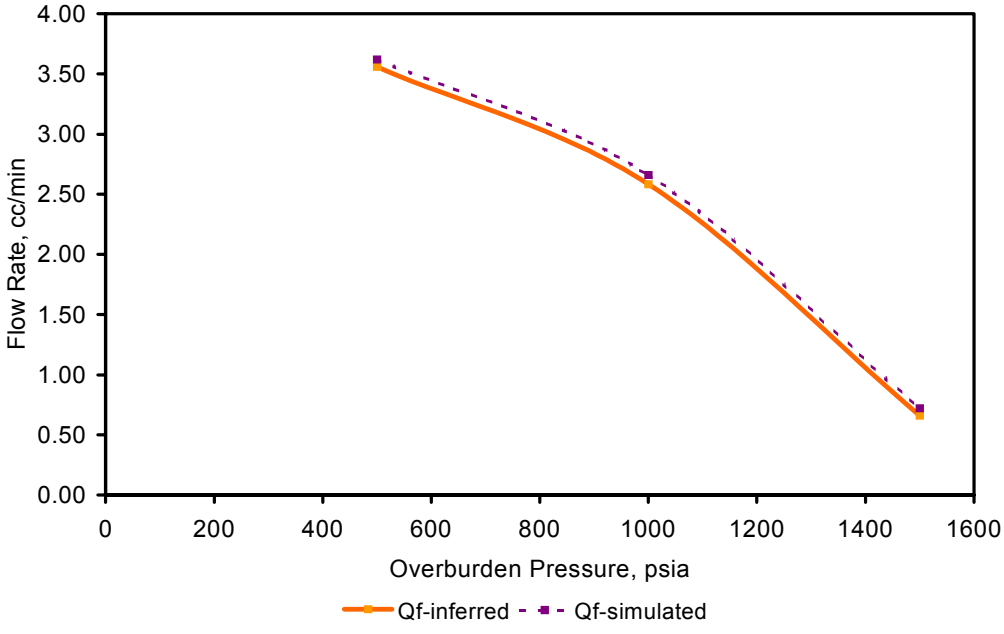

Figure 4.10 – Average fracture flow rate match between experimental data and simulated data.

Using a distributed permeability network instead of a constant permeability layer in the model, it is now possible to adequately match the experimental results. The average friction factor to obtain the match was found to be 1.25. Figures 4.8-4.10 show the results of the history match using a fracture distribution model. The matches shown are for fractured core experiments.

4.4 Simulation of X-ray CT scan experiments

In Chapter II, we had earlier described the experimental process with X–ray CT scanner. The movement of the fluid front in a region perpendicular to the fracture was observed using the X-ray CT scanner. It was also shown earlier that smooth fracture assumption failed to recreate the same movement seen through CT-scans (Fig 2.15). The fluid moved through the smooth fracture quickly because of its high permeability. Concluding that smooth fracture modeling could not replicate the movement and the average saturation calculated from CT-scans, modeling was carried out using the integrated methodology. This time the fracture apertures were distributed and accounted for roughness through a friction factor. Figure 4.11 illustrates the result of this kind of modeling.

The distributed fracture modeling also adequately matched the average water saturation inferred from X-ray CT-scans (Fig.4.12). The parallel plate model neither reproduced the movement of the water front nor matched the average water saturation obtained from the CT scans. As a result of this match, fracture aperture was estimated to be around 120 microns and the aperture distribution had a variance of 260 micron^2.

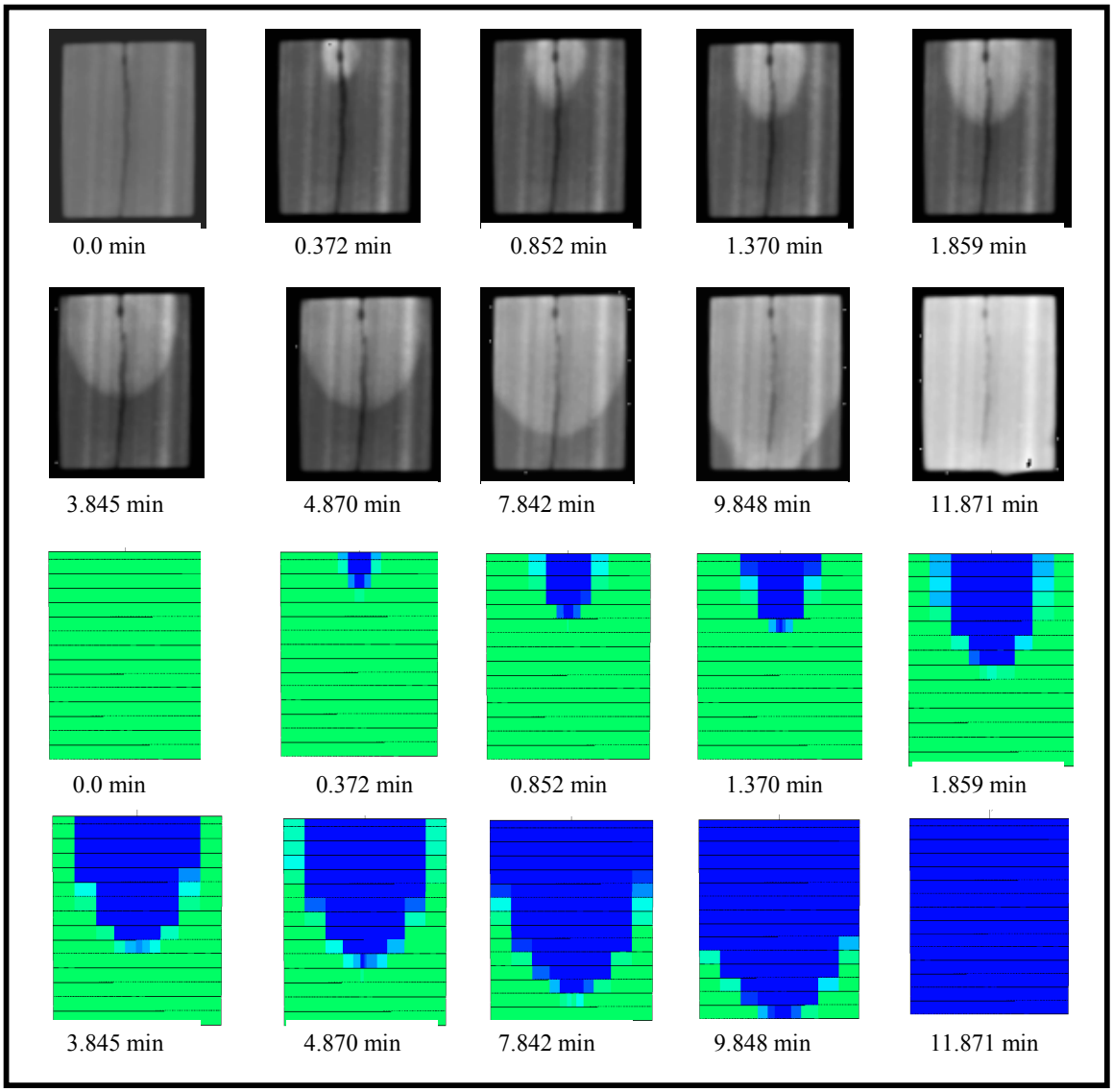

Figure 4.11 – Fluid front movement through a core with distributed fracture surface.

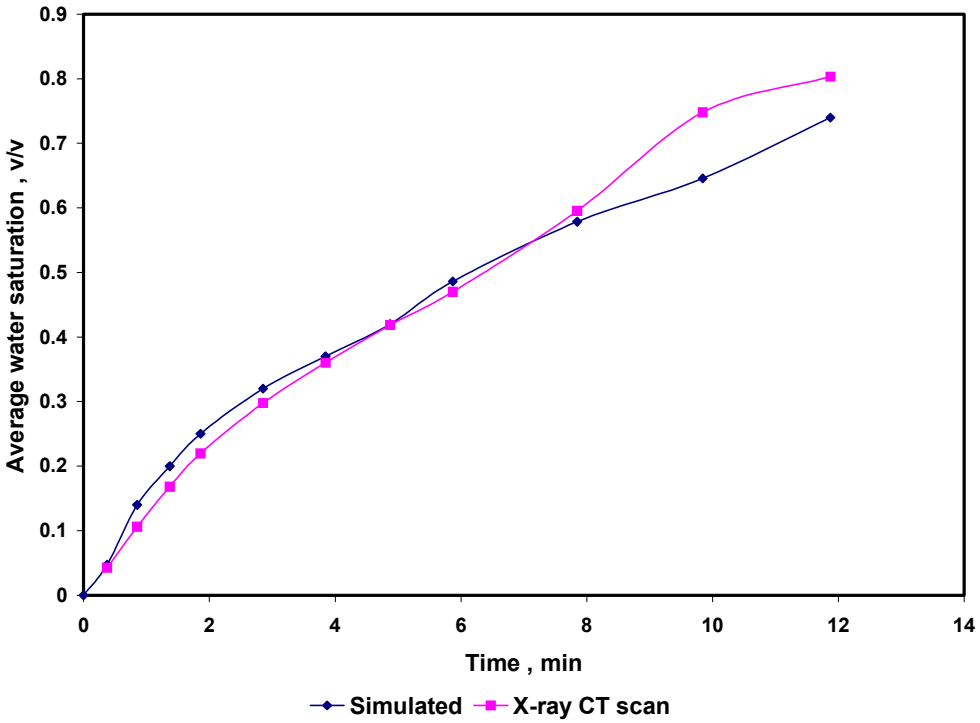

Figure 4.12 – Average water saturation match between simulation and X-ray CT scan.

4.5 Conclusions

1. The experimental observations (pressure drop across the core and flow contributions from matrix and fracture) were adequately matched using a fracture aperture distribution model.
2. The friction due to rough fracture surface was incorporated in the form of a friction factor to obtain the match.
3. The movement of the fluid front observed from X-ray CT scans was also replicated using this methodology. The parallel plate approach could not model this phenomenon.
4. Also the average water saturations calculated from CT scans were matched with a distributed aperture model.

CHAPTER V
SENSITIVITY STUDIES

5.1 Effect of variance of aperture distribution on fracture flow rate

For sensitivity studies a core model with 31x15 grid block size was used in the x and y directions with 15 layers in the z direction. The fracture layer was incorporated in the 8th layer and the rest are matrix layers. The modified permeability layer was used for the fracture layer, while the matrix layers had a constant permeability. All the layers were injected with constant water injection of 5 cc/min through injection points located at one extreme end and penetrating through all the layers. At the opposite end two production points were located, one for the matrix layers and the other for the fracture layer to quantify the amount of water produced at those two points. For this study, single phase was used.

Initially, with a constant mean aperture size of 56.4 μm, the fracture aperture distribution was generated soley through a lognormal distribution. Aperture distributions were obtained for different variances (100, 200, 600, 1000 (micron^2)). From the simulation results, it was found that the increased variance in the fracture aperture distribution leads to a reduction in the mean hydraulic aperture size. The hydraulic aperture is the value of the aperture required to produce the observed pressure drop across the core. This observation can be explained from previous observation by Dagan [35], who approximated the change in effective hydraulic aperture as a result of roughness through,

$$h_{eff}^{\ 3} \approx h_{hyd}^{\ 3}(1-1.5\ \sigma_h^{\ 2}/\langle h_{hyd}\rangle^2) \qquad (15)$$

where, h_{eff} is the effective hydraulic aperture as a result of roughness (microns) and σ_h^2 is the variance of hydraulic aperture (microns)^2 and $<h_{hyd}>$ is the mean hydraulic aperture. In our simulation experiments show the same trend as observed by Dagan. Figure 5.1 illustrates the lognormal realizations of aperture distributions with constant width and different variances while Figure 5.2 shows the comparative plots between simulated and Dagan's approximation of hydraulic aperture reduction as a result of increased roughness (variance).

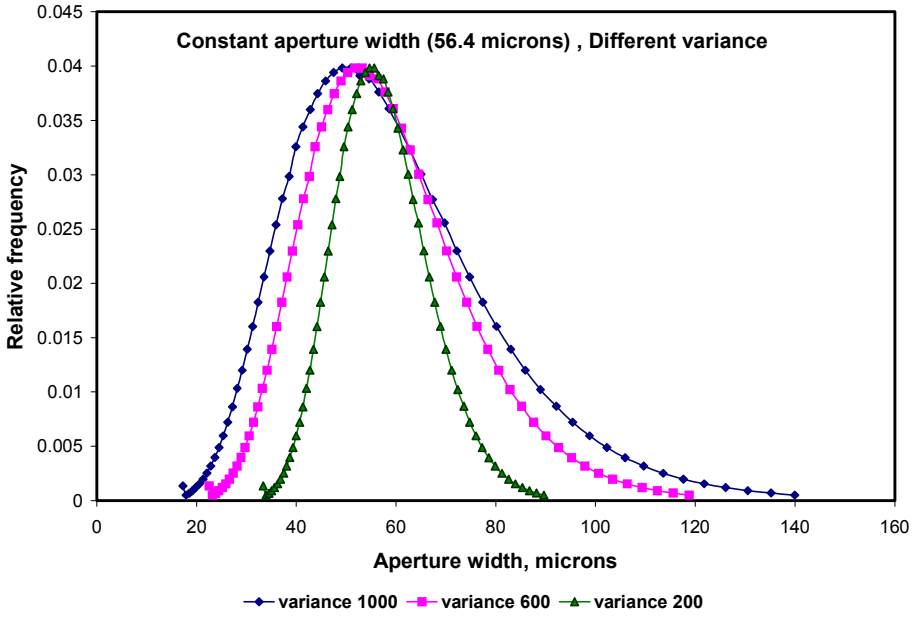

Figure 5.1 – Log-normal distribution for constant aperture width, different variances.

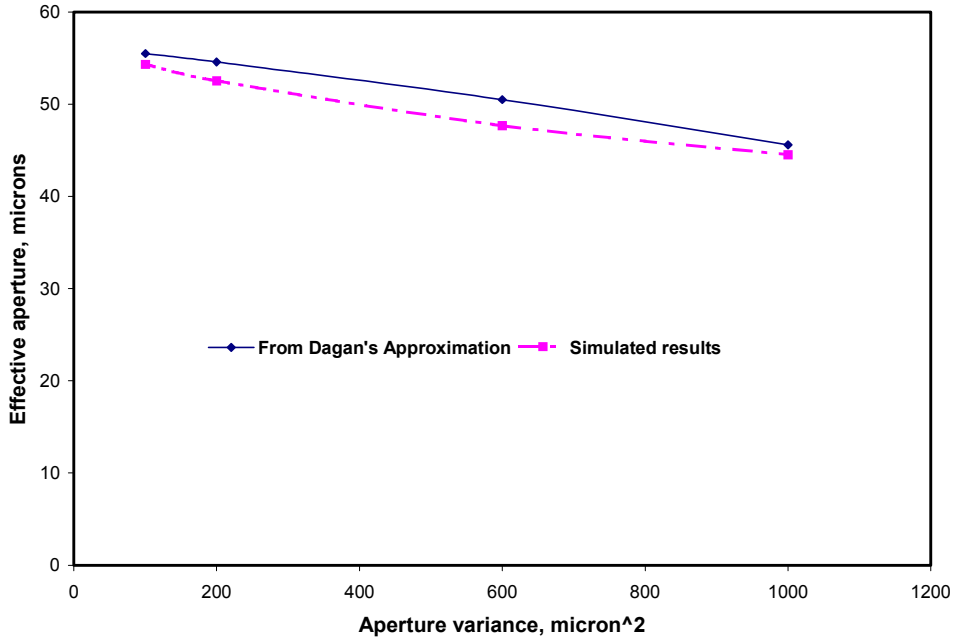

Figure 5.2 – The comparative plots of hydraulic aperture reduction as a result of increased roughness (variance) .

5.2 Determination of critical aperture size

In order to establish the limitation or restriction of this approach simulation runs were performed maintaining a constant variance and different aperture widths. Figure 5.3 illustrates the log-normal realizations of constant aperture variance but different aperture widths In other words, the aim of this sensitivity study was to determine the critical aperture width beyond which rough fracture surfaces could be treated as a smooth parallel plates. Figure 5.4 compares flow rates from fracture between the simulation runs of distributed fracture apertures accounted for roughness and parallel plate assumptions. In parallel plate assumptions, the fracture layer was assumed to be uniform rather than being distributed log-normally. Hence it had a constant permeability throughout. From the Figure it is seen that as the aperture size increases the effect of rough surfaces also gradually decreases. From the observations it is inferred that beyond an aperture size approximately 60 microns, the effects of roughness or tortuosity is found to be insignificant. This can be rooted back to the fact that larger aperture size means lower overburden pressure. So it could be inferred that as over burden pressure increases, the effect of roughness becomes more predominant.

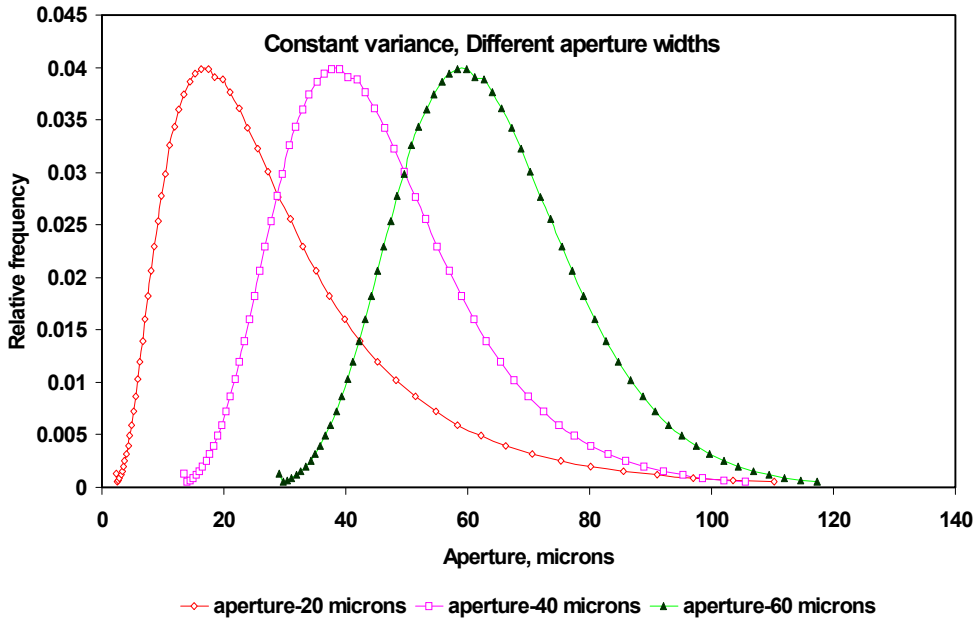

Figure 5.3 – Log-normal distribution for constant variance, different aperture widths.

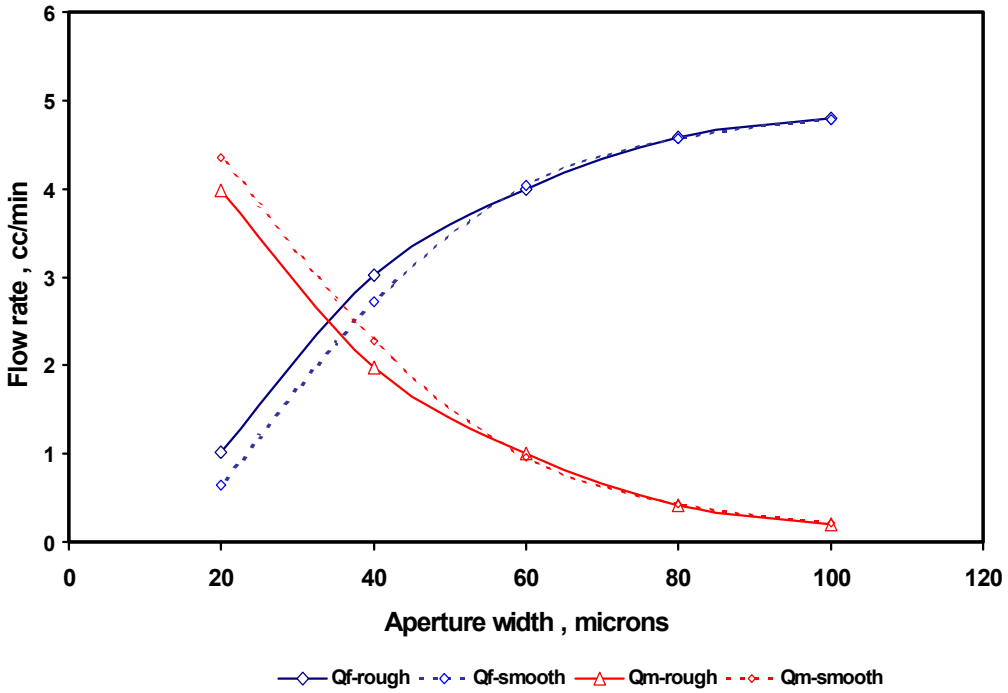

Figure 5.4 – Comparison between parallel plate (smooth) and distributed aperture flow (rough) for different apertures.

5.3 Effect of matrix permeability

The permeability of the Berea core used in the experiments is about 300 md. Usually in fractured reservoirs the matrix permeability varies in the range of 1 to 10 md. A sensitivity study was conducted to determine if matrix permeability had any impact in determining flow rates through fractures. Simulation runs were performed varying the permeability range from 0.001 to 1000 md. The size of the fracture aperture was 40 microns and the variance of the aperture distribution was 200. The injection rate of water was 5 cc/min. From the results it was inferred that only if the matrix permeability increased to beyond 1000 md, the pressure drop across the core reduced considerably. When considering a moderate permeability matrix (k = 1 md) embedded with a high fracture permeability (k ≈ 135000 md in this case), there is a significant pressure drop across the core. This pressure drop reduces significantly only when the matrix permeability increases beyond 1000 md. Figure 5.5 illustrates this phenomenon. The fracture flow rates quite naturally, also follow the same trend (Fig 5.6).

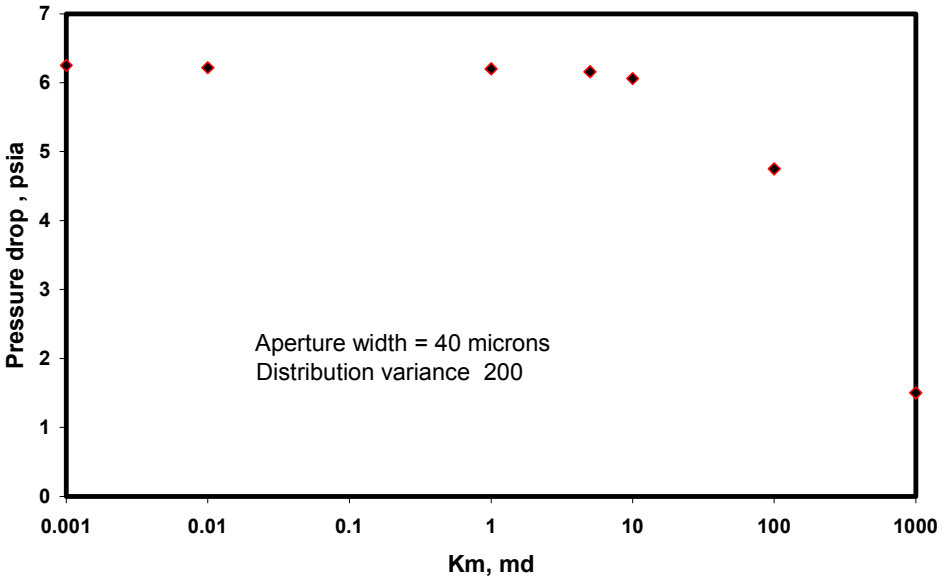

Figure 5.5– Effect of matrix permeability on pressure drop across the core.

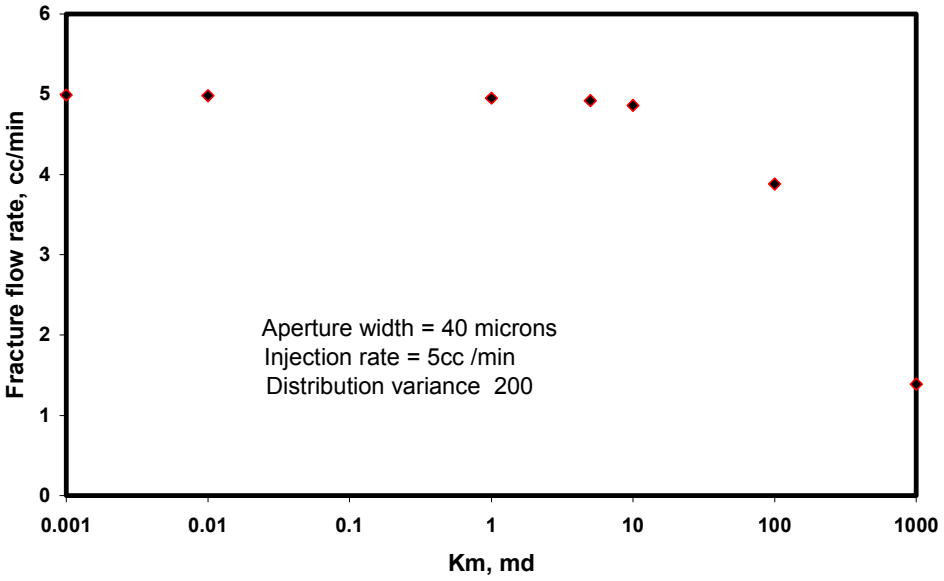

Figure 5.6 – Effect of matrix permeability on fracture flow rate.

Sensitivity studies were also conducted to observe the impact of matrix permeability between rough fracture surfaces and smooth parallel plates. Figure 5.7 compares the fracture flow rates between smooth and rough fractures for different matrix permeabilities.

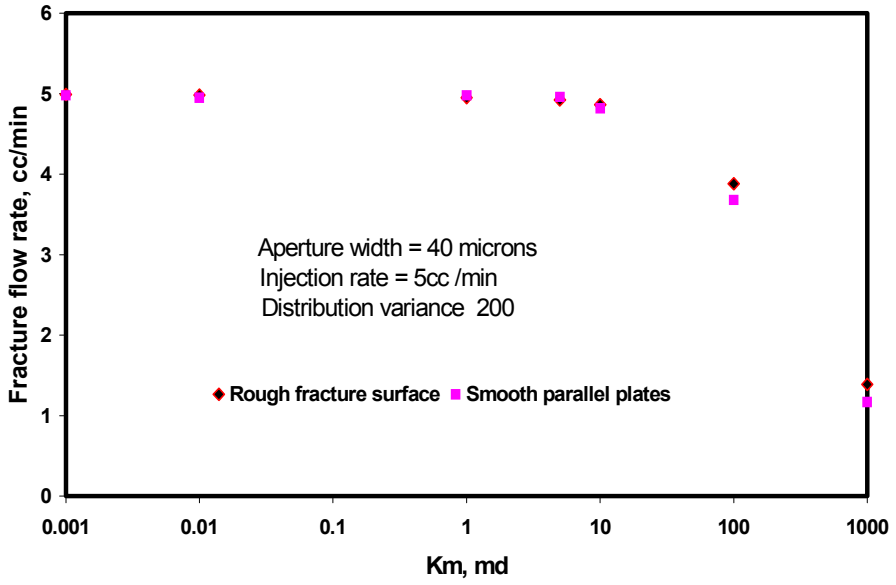

Figure 5.7 – Comparison of fracture flow rates between smooth and rough fractures for different matrix permeabilities.

Although the impact on fracture flow rates were insignificant, the effect on pressure drop was quite significant. For a range of matrix permeability between 0.001 md and 10 md, the difference in the pressure drop between rough fracture surfaces and smooth parallel plates varied from 7 to 6.2 psia. Thus distributing the fracture apertures mainly affects the pressure distribution in the core. Figure 5.8 illustrates the difference in pressure drop across the core between rough fracture and smooth fractures. The difference is almost negligible at a matrix permeability of 1000 md. But in reality we seldom find a reservoir with high matrix permeability like that.

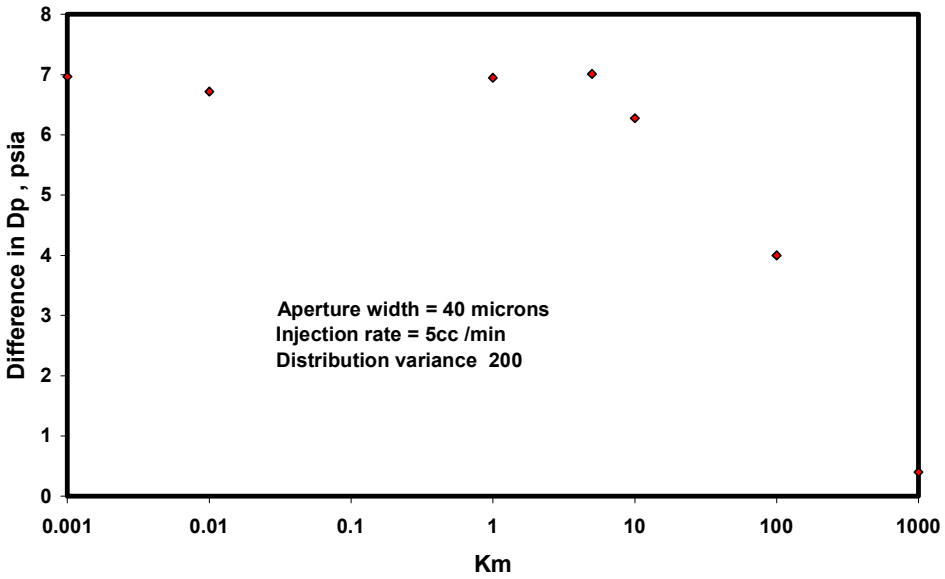

Figure 5.8 – Difference in pressure drop across the core between smooth and rough fractures at different matrix permeabilities.

5.4 Effect of matrix heterogeneity

In the core experiments the berea core was used. The berea core is known to be fairly homogeneous core with high matrix permeability. The true effect of matrix heterogeneity can only be established after having studied the core with an X-ray CT scanner. The porosity distribution of the core can be established through CT scans. But for permeability distribution some kind of empirical correlation has to be used, since matrix permeability heterogeneity cannot be established through CT scans. In this research an attempt was made to study the effect of matrix heterogeneity on flow through the fractures. Two cases were run to study the effect. The first case had a single value for matrix permeability (100 md) and in the second case the matrix permeabilities were distributed randomly in the range of 80 to 130 md. In both the cases the fracture permeability layer was distributed through the lognormal distribution (mean aperture = 60 microns and variance = 500 micron ^{2}). Figures 5.9 and 5.10 show the distribution of permeabilities used in the matrix (case 2) and the fracture layer respectively.

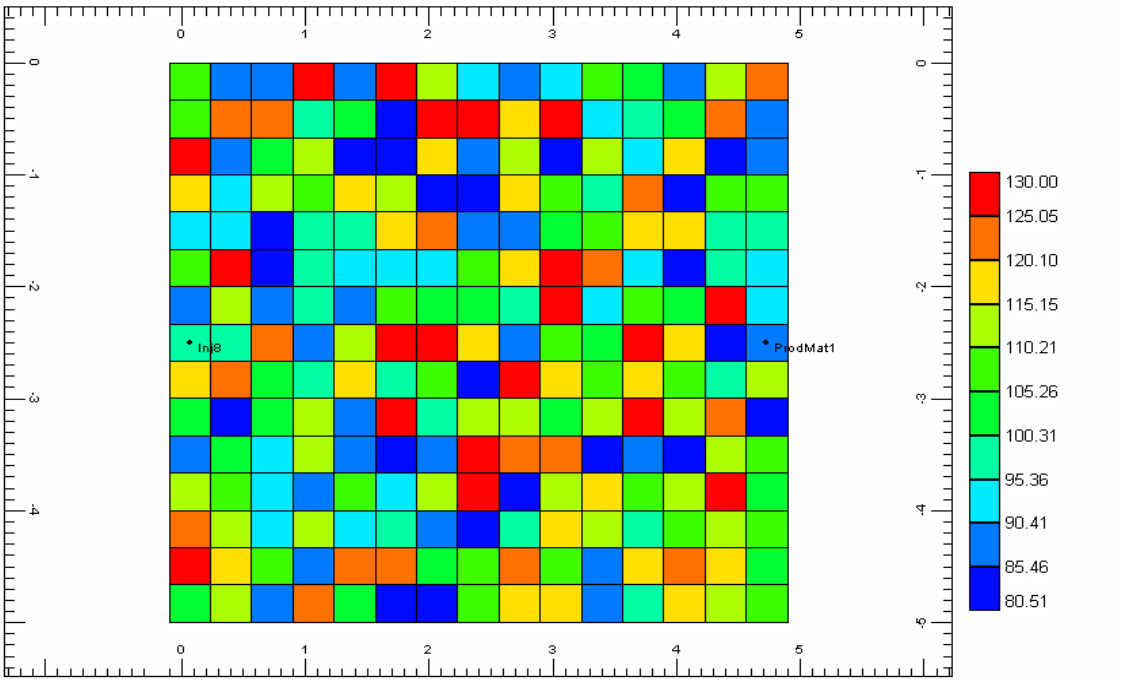

Figure 5.9 – Distribution of matrix permeability layer (case 2).

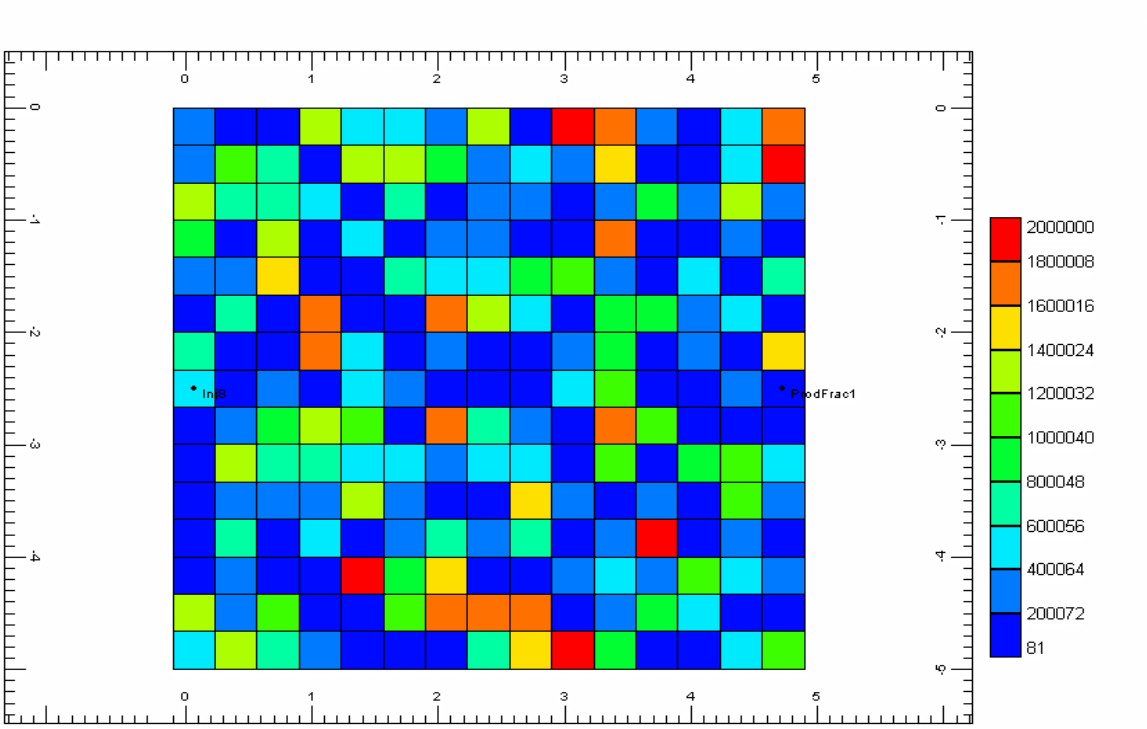

Figure 5.10 – Distribution of fracture permeability layer (cases 1 and 2).

The total area of the matrix in this study was 5 cm * 5 cm * 5 cm. The simulation grid size used was 15*15*15. The fracture layer was introduced in the 8th layer in the z-direction. An injection rate of 5 cc/min was applied at one end and was produced at the other end. The fracture flow rates obtained from both the cases were 3.76 cc/min (case 1) and 3.82 cc/min (case 2). The difference in the flow rates was 0.04 cc/min, which is about 1% change from the case of constant matrix permeability. Thereby, matrix heterogeneity of a core with high matrix permeability (100 md in this case) does not play a significant role in affecting flow contributions through a fracture.

5.5 Simulator testing

Sensitivity studies were also performed to test whether the simulator provides accurate results when confronted with a very high permeability region (fracture) among surrounding matrix blocks (low permeability regions). A one-dimensional model was established in which serial flow was modeled across blocks of moderate permeability (10 md) with a high permeability block embedded in the centre. The values for high permeability were varied from 100 md to 10000000 md. An example of the model is shown in Fig. 5.11, where the value of the high permeability region is 10000 md. The model was injected from one end and produced at the other end. The injection rate used in this case was 5 cc/min. The producer was operated at atmospheric pressure. The pressure drop obtained from simulations were compared with those obtained from Darcy's law. The pressure drop across the core is obtained from Darcy's law through,

$$\Delta p = \frac{Q * \mu * l}{\bar{k} A} \tag{21}$$

where Q is the matrix flow rate (cc/sec), $\bar{k}$ is the average matrix permeability (Darcy), A is the matrix area (cm^2), Δp is pressure drop across the core (atm), μ is viscosity (cp) and L is core length (cm).

The average permeability $\bar{k}$ for this model can be obtained through [36],

$$\bar{k} = \frac{L}{\sum \frac{l_i}{k_i}} \tag{22}$$

where L is the total length of the core, l_i is the length of the grid block (x-dir) and k_i is the corresponding grid block permeability.

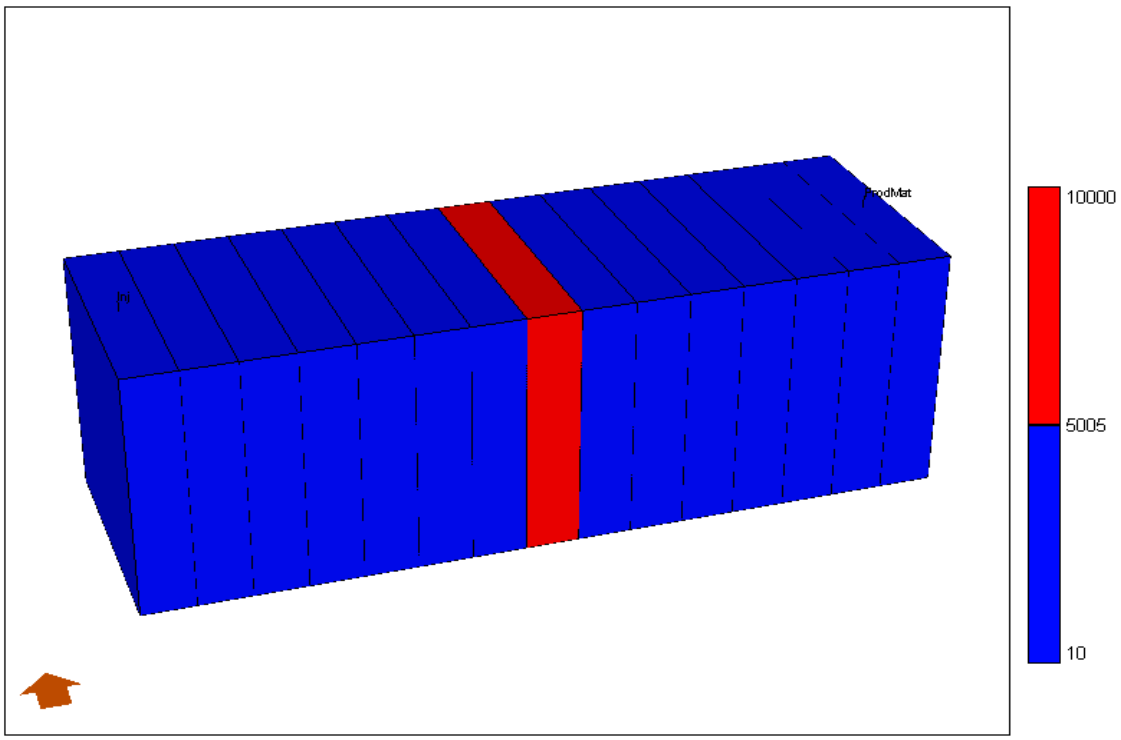

Figure 5.11 – One-dimensional model employed in simulation testing.

The results of simulation testing are given in Fig. 5.12. The pressure drops obtained from simulation are compared with those obtained from Darcy's law. The comparison shows the values obtained from simulation are consistent with Darcy's law.

The maximum deviation was about 0.25 psi, which is less than 1% of the actual value. Accurate results can be obtained from increased griding.

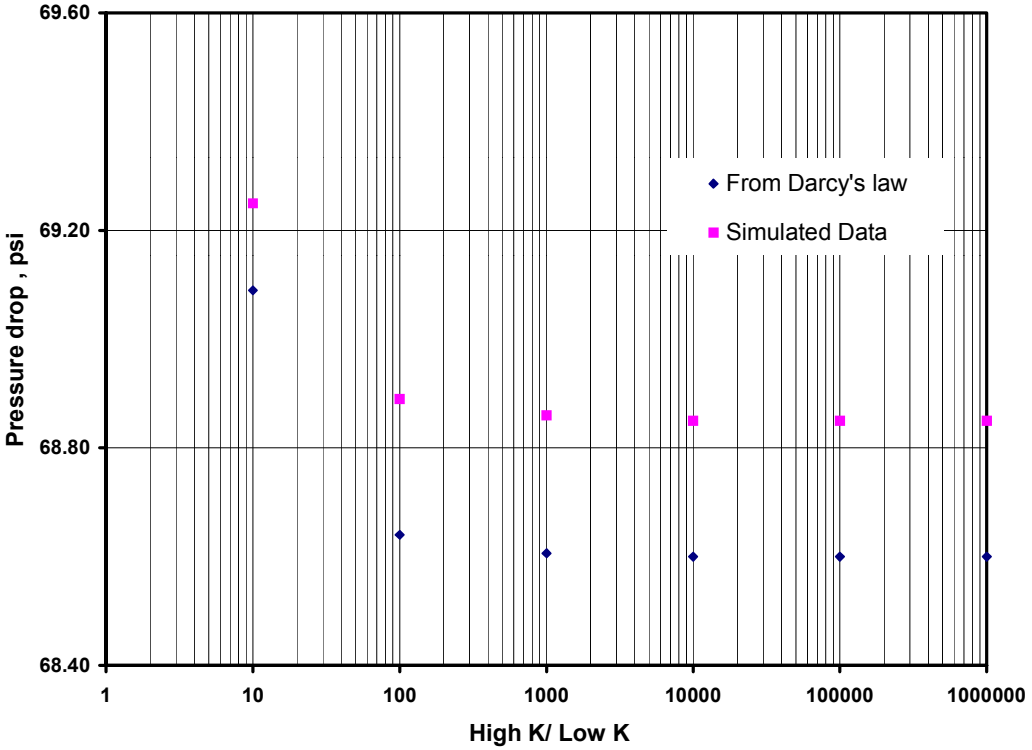

Figure 5.12 – Comparative plot of pressure drops observed from simulation and through Darcy's law.

5.6 Conclusions

1. The effective hydraulic aperture is reduced with increased variance of the aperture distribution.
2. Beyond an aperture size of approximately 60 microns, the effects of roughness or tortuosity is found to be insignificant.
3. The sensitivity studies on matrix permeability show that the fracture has to be modeled with a two dimensional aperture distribution regardless of the value of

matrix permeability. Even though the flow rates may appear to be the same, the pressure drop across the core is different.

4. Matrix heterogeneity in cores with high permeability do not affect the flow rate through fracture significantly.
5. The simulator is found to give consistent results when embedded with a region of very high permeability among moderate permeability blocks.

CHAPTER VI

DISCUSSION AND CONCLUDING REMARKS

Even though much work has yet to be accomplished to have all the necessary analysis and data to provide a detailed modeling procedure for flow through single fractures, the proposed methodology is able to model flow experiments through single fractures fairly well. So far, the following conclusions can be drawn based on the work.

1. Quantification of effective aperture widths is possible through proper design of experiments.
2. From simulation observations it is found that fracture aperture needs to be distributed to accurately model the experimental results.
3. The effect of friction due to surface roughness needs to be taken into account while modeling. In these experiments friction reduced the flow through the fractures by approximately 24%. In addition to the reduction of flow, the pressure drop observed across the core is quite different from the one that would result due to smooth parallel plates.
4. There is an increased flow though fractures when the variance of the aperture distribution is increased. This reiterates the fact that tortuosity in fluid flow is a significant factor.
5. Though it is shown that effective aperture successfully modeled experimental results using the integrated methodology, the value of the fracture aperture is only a close estimate. The correct value of the fracture aperture can be obtained with high accuracy using an X-Ray CT Scan.
6. This methodology could be effectively utilized for large field scale modeling for fractured reservoirs, where the practice of using a constant permeability layer to model fracture layer exists. In this work it is shown that though constant permeability layer could match the flow rate and pressure drop across the core individually; the possibility of matching both simultaneously is very remote.

Modeling flow through fractures is an area of active research. The methodology described in this work could open more perspectives in fracture modeling. Improvements could be made to this model by distributing porosity in the core scale and also considering the effect of matrix heterogeneity. Our next step would be to apply this methodology to two-phase flow and also upscaling from core scale to field scale.

NOMENCLATURE

A = matrix area (cm^2)

f = friction factor

k_m = matrix permeability (Darcy)

k_f = fracture permeability (Darcy)

L = core length (cm)

l = diameter of the core (cm)

q_m = matrix flow rate (cc/sec)

q_f = fracture flow rate (cc/sec)

w = effective fracture width (cm)

Δp = pressure drop across the core (atm)

μ = viscosity (cp)

REFERENCES

1. Iwai, K.: “Fundamental studies of fluid flow through a single fracture,” Ph.D. dissertation, University of California. Berkeley, CA (1976).
2. Putra, E., Fidra, Y., and Schechter, D.S.: “Study of Waterflooding Process in Naturally Fractured Reservoirs from Static and Dynamic Imbibition Experiments,” paper SCA 9910 presented at the 1999 International Symposium of the Society of Core Analysts, Colorado, 1-4 August.
3. Lee, J. and Kang, J.M.: “Oil Recovery in a Fracture of Variable Aperture With Countercurrent Imbibition: Experimental Analysis,” paper SPE 56416 presented at the 1999 Annual Technical conference and Exhibition, Houston, Texas, 3-6 October.
4. Murphy, J.R. and Thomson, N.R.: “Two-Phase Flow in a Variable Aperture Fracture,” *Water Resources Research* (1993), **29**, No. 10, 3453.
5. Persoff, P. and Pruess, K.: “Two-Phase Flow Visualization and Rough-Walled Rock Fractures,” Water Resources Research (1993), **31**, No. 5, 1175.
6. Firoozabadi, A. and Tan, J.C.T: “Miscible Displacement in Fractured Porous Media: Part A -Analysis,” paper SPE/DOE 27837 presented at the 1994 SPE/DOE Ninth Symposium, Tulsa, OK, 17-20 April.
7. Lomize, G.M.: *Seepage in Fissured Rocks*, State Press, Moscow (1951)
8. Snow, D.T.: “Anisotropic Permeability of Fractured Media,” *Water Resources Research* (1969), **5**, No. 6, 1173-1189.
9. Neuzil, C.E., and Tracy, J.V.: “Flow Through Fractures,'” *Water Resources Research* (1981), **17**, No. 1, 191-199.
10. Witherspoon, P. A., Wang, J. S. Y., Iwai, K. and Gale, J. E.: “Validity of Cubic Law for Fluid Flow in a Deformable Rock Fracture, *Water Resources Research* (1980), **16**, No. 6, 1016-1024.
11. Tsang, Y.W. and Witherspoon, P.A.: 'The Dependence of Fracture Mechanical and Fluid Flow Properties on Fracture Roughness and Sample Size,” *Journal of Geophysical Research* (1983), **88**, No. 3, 2359-2366.

12. Bandis, S., Lumisden, A.C. and Barton, N.R.: "Experimental Studies of Scale Effects on the Shear Behavior of Rock Joints," *Int. J. Rock Mech. Min. Sci*. (1981), **18**, 1-21.
13. Tsang, Y.W., Tsang, C.F., Neretnieks, I. and Moreno, L.: "Flow and Transport in Fractured Media: A Variable Aperture Channel Model and Its Properties," *Water Resources Research* (1988), **24**, No. 12, 2049-2060.
14. Brown, S.R.: "Fluid Flow Through Rock Joints: The Effect of Surface Roughness," *Journal of Geophysical Research* (1987), **92**, No. B2, 1337-1347.
15. Tsang, Y.W. and Tsang, C.F.: "Channel Model of Flow Through Fractured Media," *Water Resources Research* (1987), **23**, No. 3, 467-479.
16. Moreno, L., Tsang, Y.W., Tsang, C.F., Hale, F.V. and Neretnieks, I.: "Flow and Tracer Transport in a Single Fracture: A Stochastic Model and Its Relation to Some Field Observations," *Water Resources Research* (1988), **24**, No. 12, 2033-2048.
17. Tsang, Y.W. and Tsang, C.F.: " Flow Channeling in a Single Fracture as a Two-Dimensional Strongly Heterogeneous Permeable Medium," *Water Resources Research* (1989), **25**, No. 9, 2076-2080.
18. Tsang, Y.W., Tsang, C.F., Neretnieks, I., Moreno, L.: "Flow and Tracer Transport in Fractured Media: A Variable Aperture Channel Model and Its Properties," *Water Resources Research* (1988), **24**, No. 12, 2049-2060.
19. Fatt, I. and Davis, D.H.: "Reduction in Permeability with Overburden Pressure," *Trans.*, AIME (1952),**195**, 329.
20. Wyble, D.O.: "Effect of Applied Pressure on the Conductivity, Porosity and Permeability on Sandstones," *Trans.*, AIME (1958) **213**, 430.
21. Gray H. D., Fatt, I., and Bergamini, G.: "The Effect of Stress on Permeability of Sandstone Cores," *SPEJ* (June 1963), 49.
22. Lorenz, J.C.: "Stress-Sensitive Reservoirs," *JPT* (Jan 1999), 61.
23. Jin, M., Somerville, J. and Smart, B.G.D.: "Coupled Reservoir Simulation Applied to the Management of Production Induced Stress-Sensitivity," paper SPE 64790 presented at the 2000 International Oil and Gas Conference and Exhibition, Beijing, China, Nov 7-10.

24. Atkinson, B. K.: *Fracture Mechanics of Rock*, Academic Press, New York (1989), 548.
25. Lawn, B. R. and Wilshow, T. R.: *Fracture of Brittle Soils*, Cambridge University Press, Cambridge (1975).
26. Palmer, I. D. and Sparks, D. P.: "Measurement of Induced Fractures by Downhole TV Camera in Black Warrior Basin Coalbeds," *JPT* (1991), **43**, No. 3, 270.
27. Overbey, W. K., Yost, L. E. and Yost, A. B.: "Analysis of Natural Fractures Observed by Borehole Video Camera in a Horizontal Well," paper SPE 17760 presented at the 1988 SPE Gas Technology Symposium, Dallas, 13-15 June.
28. National Research Council: *Rock Fracture and Fracture Flow: Contemporary Understanding and Applications*, Committee on Fracture Characterization and Fluid Flow, National Academy Press, Washington, D. C. (1996).
29. Brown, A. R., Kranz, R. L. and Bonner, B. P.: "Correlation between the Surfaces of Natural Rock Joints*," Geophysical Research Letters* (1986), **13**, No. 13, 1430-1433.
30. Brown, A. R. and Scholz, C. H.: "Broad Bandwidth Study of the Topography of Natural Rock Surfaces," *Journal of Geophysical Research* (1985), **90**, No.B14, 12575-12582.
31. Gale, J. E.: "Comparison of Coupled Fracture Deformation and Fluid Flow Models with Direct Measurement of Fracture Pore Structure and Stress-Flow Properties," *Proceedings of the 28th U. S. Symposium of Rock Mechanics* (1987), 1213-1222
32. Pyrak-Nolte, L.J., Myer, L.R. and Witherspoon, P.A.: Hydraulic and Mechanical Properties of Natural Fractures in Low Permeability Rock, *Proceedings of the 6th International Congress of Rock Mechanics,* Montreal, Canada (1987), 225-231.
33. Shimo, M. and Long, J.C.S.: "A Numerical Study of Transport Parameters in Fracture Networks," *Flow and Transport through Unsaturated Fractured Rock*, D.D. Evans and T.J. Nicholson (editors), American Geophysical Union Monograph (1987), **42,** 127-135.
34. Davis, J. C. (Ed.), *Statistics and Data Analysis in Geology*, John Wiley, New York (1986), 646.

35. Zimmerman R.W. and Bodvarsson, G.S.: "Hydraulic Conductivity of Rock Fractures" *Transport in Porous Media* (1996), **23**, 1-30.

APPENDIX A
PROCEDURES FOR CONDUCTING CORE FLOODING EXPERIMENTS AND PRECAUTIONS

For single phase experiments:

1. Wash the core before saturating the core at about 350°C temperature for about two days.
2. Saturate the core before starting the experiment for about two days.
3. Make sure the two valves between the pumps and the accumulators are turned off before refilling the pumps.
4. Obtain the desired overburden pressure using hydraulic jack. This may cause several attempts to stabilize, as there will be air trapped in line causing you to lose overburden pressure.
5. Fill brine in accumulator 1 and kerosene or oil in accumulator 2, if necessary.
6. Turn on the valve between the pump 1 and the accumulator 1, and turn the valves to on position on the permeameter.
7. Turn the red valve to on position, which connects accumulator 1 to the core holder. Make sure that the black valve connecting accumulator 2 and core holder is off.
8. Perform the core flooding experiment with different flow rates and note the pressure difference in the permeameter.
9. Change the overburden pressure and perform the experiment and note the readings.
10. Fracture the core and place it again in the core holder and apply overburden pressure. Close the black valve and open the red valve again and perform the core flooding experiment with brine. Note the readings.

Precautions:

1. Filter the brine to avoid any dissolved solids that choke the core.
2. Make sure the experiment is performed without any air trapped in the core.
3. While refilling the accumulators, care should be taken to close the valves between accumulator and core holder to avoid any air entering the pipelines.
4. Fracture the core as soon as possible to avoid much loss of fluid.
5. Note the volume of outlet pipeline from the core holder and subtract it from the amount of brine discharged while kerosene is injected.
6. After each flow, allow the pressure to drop close to atmospheric pressure before starting the next flow.

VITA

Dicman Alfred holds a B.Tech. degree in mechanical engineering from the Indian Institute of Technology, Madras. Prior to joining TAMU he worked as logging engineer with Halliburton Energy Services. He was involved in the U.S Department of Energy sponsored pilot project "Investigation of Efficiency Improvements during CO2 Injection in Hydraulically and Naturally Fractured Reservoirs." His research areas include wireline-logging, formation evaluation, numerical modeling/reservoir simulation and reservoir engineering.

His current address: Texas A&M University

Attn.: Dr. David S. Schechter

Harold Vance Department of Petroleum Engineering

3116 TAMU

College Station, TX 77843-3116

USA